HHS Public Access

Author manuscript

Neuroimage. Author manuscript; available in PMC 2022 August 08.

Published in final edited form as:

Neuroimage. 2020 March ; 208: 116406. doi:10.1016/j.neuroimage.2019.116406.

Diffusion Kurtosis Imaging maps neural damage in the EAE model of multiple sclerosis

Andrey Chuhutin[a,*], **Brian Hansen**[a], **Agnieszka Wlodarczyk**[b], **Trevor Owens**[b], **Noam Shemesh**[c], **Sune Nørhøj Jespersen**[a,d]

[a]CFIN, Aarhus University, Aarhus, Denmark

[b]Department of Neurobiology Research, Institute for Molecular Medicine, University of South Denmark, Odense, Denmark

[c]Champalimaud Research, Champalimaud Centre for the Unknown, Lisbon, Portugal

[d]Department of Physics, Aarhus University, Aarhus, Denmark

Abstract

Diffusion kurtosis imaging (DKI) is an imaging modality that yields novel disease biomarkers and in combination with nervous tissue modeling, provides access to microstructural parameters. Recently, DKI and subsequent estimation of microstructural model parameters has been used for assessment of tissue changes in neurodegenerative diseases and associated animal models. In this study, mouse spinal cords from the experimental autoimmune encephalomyelitis (EAE) model of multiple sclerosis (MS) were investigated for the first time using DKI in combination with biophysical modeling to study the relationship between microstructural metrics and degree of animal dysfunction. Thirteen spinal cords were extracted from animals with varied grades of disability and scanned in a high-field MRI scanner along with five control specimen. Diffusion weighted data were acquired together with high resolution T_2* images. Diffusion data were fit to estimate diffusion and kurtosis tensors and white matter modeling parameters, which were all used for subsequent statistical analysis using a linear mixed effects model. T_2* images were used to delineate focal demyelination/inflammation. Our results reveal a strong relationship between disability and measured microstructural parameters in normal appearing white matter and gray matter. Relationships between disability and mean of the kurtosis tensor, radial kurtosis, radial diffusivity were similar to what has been found in other hypomyelinating MS models, and in patients. However, the changes in biophysical modeling parameters and in particular in extra-axonal axial diffusivity were clearly different from previous studies employing other animal

*Corresponding author. andrey@cfin.au.dk (A. Chuhutin).

Author contribution

Andrey Chuhutin: Investigation, Formal analysis, Software, Data Curation, Writing - Original Draft, Writing - Review & Editing, Visualization.

Brian Hansen: Conceptualization, Writing - Review & Editing, Supervision.

Agnieszka Wlodarczyk: Investigation, Resources.

Trevor Owens: Methodology, Project administration, Resources.

Noam Shemesh: Resources, Investigation, Writing - Review & Editing.

Sune Nørhøj Jespersen: Conceptualization, Supervision, Writing - Review & Editing, Methodology.

Appendix A. Supplementary data

Supplementary data to this article can be found online at https://doi.org/10.1016/j.neuroimage.2019.116406.

models of MS. In conclusion, our data suggest that DKI and microstructural modeling can provide a unique contrast capable of detecting EAE-specific changes correlating with clinical disability.

Keywords

Diffusion MRI; WMM; EAE; DKI; Multiple sclerosis; White matter modeling; Kurtosis

1. Introduction

Multiple sclerosis (MS) is a demyelinating, inflammatory, neurodegenerative disease of the human central nervous system (CNS) affecting millions of people worldwide. The pathophysiology of MS is often complex, and involves, among other factors, myelin loss, axonal damage, appearance of transient or permanent lesions, and brain atrophy. Effective treatment of MS is still lacking (Compston and Coles, 2002), although a range of disease-modifying therapies have been introduced (Berger, 2011; Noyes and Weinstock-Guttman, 2013). These therapies are based on immunomodulatory, anti-inflammatory, and immunosuppressive drugs. The success of such treatments depends on early diagnosis and careful monitoring of the patient.

A range of MS animal models characterized by different mechanisms of induction and pathology (Lassmann and Bradl, 2016) have been developed to overcome the limitations of clinical tissue assessment. Experimental autoimmune encephalomyelitis (EAE) is a group of the most compelling and commonly used animal MS models (Baker and Amor, 2014; Kipp et al., 2016; Lassmann and Bradl, 2016). Unlike other animal models, in addition to inflammatory lesions and demyelination, EAE includes axonal damage (Bergers et al., 2002; Kipp et al., 2016) which is one of the hallmarks of MS. Therefore, using EAE to assess MS biomarkers can provide unique insights into the MS pathology.

Due to its noninvasiveness and ability to contrast soft tissues, Magnetic Resonance Imaging (MRI) is extensively used for diagnosis and monitoring of MS (Bakshi et al., 2008; Polman et al., 2011). Standard T_1- or T_2-weighted MRI images are capable of revealing brain atrophy and lesions, which are heterogeneous areas harboring demyelination, inflammation, gliosis and axonal injury (Filippi et al., 2012; Inglese and Bester, 2010). However, diffuse microstructural changes outside the T_1 or T_2 intensity lesions in gray matter (GM) and so-called normal appearing white matter (NAWM) (Allen et al., 2001) have been observed with histology. Studies (De Stefano et al., 2006; Kipp et al., 2016; Miller et al., 2003) showed that the diffuse damage in NAWM and GM contributes to disability accumulation and chronic disease progression.

Diffusion weighted imaging (DWI) can provide quantitative microstructural information by sensitizing MRI signals to the displacement of water molecules. The underlying signal attenuation is often approximated by a Gaussian distribution, which forms the basis of diffusion tensor imaging (DTI) (Basser and Pierpaoli, 1996). While DTI metrics are widely used, the mentioned Gaussian approximation is valid only in a limited regime of low diffusion weighting. At higher gradient strengths (or b-values), tissue microstructure and compartmentalization cause deviations from Gaussianity. These deviations are utilized by

a framework known as diffusion kurtosis imaging (DKI) (Jensen et al., 2005; Jensen and Helpern, 2010). Combined with tissue modeling, DKI provides access to microstructural parameters and yields novel disease biomarkers.

DKI based biomarkers have been shown to improve the diagnostic assessment in a range of neurological disorders (Delgado y Palacios et al., 2014; Grossman et al., 2011; Khan, 2016; Surova et al., 2016; Tietze et al., 2015; Wang et al., 2011). In MS, they improved characterization of GM and NAWM damage (Raz et al., 2013; Yoshida et al., 2013) and correlated with cognitive impairment (Bester et al., 2015). In MS animal models, DKI biomarkers were associated with chronic injury (Falangola et al., 2014; Guglielmetti et al., 2016; Jelescu et al., 2016) and neurite myelin content (Kelm et al., 2016). However, even though (Wu and Cheung, 2010) employed EAE to show that DKI is able to enhance lesion detection and other DWI methods revealed pathological changes in EAE (Biton et al., 2005; Budde et al., 2009), DKI and white matter (WM) models have never been used to investigate EAE-induced disability.

In this study, we hypothesized that novel metrics obtained using DKI could predict the EAE disability. If this hypothesis is found to be true, and provided our methods are successfully translated to clinic setting, the results of this study can support usage of DKI-derived biomarkers as a diagnostic tool for MS. A detailed description of the chosen DKI-derived metrics is provided in the next chapter following the definition of the metrics and a description of their relationship to the pathology.

The ability of DKI to provide quantitative biomarkers of dysfunction in EAE model of MS was investigated by testing the correlation between the biomarkers and behavioral markers of disease severity. Inside lesions no biomarkers showed correlation to disability. In NAWM, the DKI parameters showed better correlation to disability than DTI, suggesting that changes in kurtosis parameters may precede lesion formation. Standard DKI and DTI parameters produced results similar to those shown previously in other MS models. The estimated parameters of the WM model, however, yielded new microstructural information that could provide a key for improved understanding of EAE mechanisms.

2. Methods

2.1. Theory. Diffusion Kurtosis Imaging

DKI (Jensen et al., 2005) improves the approximation of the diffusion weighted signal in vivo (Filli et al., 2014; Raz et al., 2013; Rosenkrantz et al., 2015) and ex vivo (Veraart et al., 2011) by including the next term in the cumulant expansion (Kiselev, 2010; van Kampen, 2007) of the DWI signal S

$$\log S(b,\hat{\mathbf{n}}) = -b\sum_{i,j=1}^{3} D_{i,j}\hat{\mathbf{n}}_i\hat{\mathbf{n}}_j + \frac{b^2\overline{D}^2}{6}\sum_{i,j,k,l=1}^{3} W_{i,j,k,l}\hat{\mathbf{n}}_i\hat{\mathbf{n}}_j\hat{\mathbf{n}}_k\hat{\mathbf{n}}_l \quad (1)$$

where $D_{i,j}$ is the i,j element of the rank 2 symmetric diffusion tensor $\mathbf{D}$ and $W_{i,j,k,l}$ is the i,j,k,l element of the symmetric rank 4 kurtosis tensor $\mathbf{W}$, b is the diffusion weighting (b-value), $\overline{D} = \mathrm{Tr}(\mathbf{D})/3$ and $\hat{\mathbf{n}}_i$ denotes the i-th component of measurement direction $\hat{\mathbf{n}}$. In

analogy to diffusion tensor based fractional anisotropy (FA), mean (MD), axial ($D_\parallel$) and radial ($D_\perp$) diffusivity, the kurtosis tensor ($\mathbf{W}$) provides additional biomarkers: kurtosis fractional anisotropy (KFA) (Hansen and Jespersen, 2016), mean of the kurtosis tensor (MKT) (Hansen et al., 2014, 2013) (MKT = Tr($\mathbf{W}$)/5), axial ($K_\parallel$) and radial 5 kurtosis ($K_\perp$) (Jensen and Helpern, 2010).

The choice of the DTI parameters assessed in this study was based on previous works. In particular, FA, MD, $D_\parallel$ and $D_\perp$ have been shown to be affected by MS pathology (Ceccarelli et al., 2007; de Kouchkovsky et al., 2016; Falangola et al., 2014; Guglielmetti et al., 2016; Inglese and Bester, 2010; Jelescu et al., 2016; Kelm et al., 2016; Mesaros et al., 2009). In DKI, a choice of MKT was motivated by a decrease in mean kurtosis that was shown in human GM and NAWM (Raz et al., 2013; Yoshida et al., 2013) and linked with cognitive impairment in MS (Bester et al., 2015). A decrease in axial kurtosis $K_\parallel$ and radial kurtosis $K_\perp$ was detected in an animal model of chronic MS (Falangola et al., 2014; Guglielmetti et al., 2016), $K_\perp$ was found to be related to the myelin content (Kelm et al., 2016).

In this work, we used a variant of the ‘standard’ WM model (WMM) that has been extensively explored recently (Fieremans et al., 2011; Jelescu et al., 2015a; Jespersen et al., 2007; Novikov et al., 2018b; Zhang et al., 2012). The model is designed to approximate diffusion inside and outside WM fascicles. It consists of two non-exchanging Gaussian compartments representing extra-axonal and intra-axonal space. Here, the diffusion in the extra-axonal space is described by an anisotropic cylindrically symmetric tensor which is defined by extra-axonal radial and axial diffusivities ($D_{e,\perp}$ and $D_{e,\parallel}$). Axons, having radii much smaller than the diffusion distance, are assumed to appear as one-dimensional sticks and thus only the intra-axonal axial diffusivity D_a is non-vanishing. Taking f to be the volume fraction of the axonal compartment, and $\mathcal{P}(\hat{\mathbf{u}})$ to be the fiber-orientation distribution function (fODF), the diffusion signal S measured in the direction can be written as:

$$S(b,\hat{\mathbf{n}}) = \int \mathrm{d}\hat{\mathbf{u}}\mathcal{P}(\hat{\mathbf{u}})\Big(f\exp\Big(-bD_a(\hat{\mathbf{u}}\cdot\hat{\mathbf{n}})^2\Big) + (1-f)\exp(-bD_{e,\perp} - b\big(D_{e,\parallel} - D_{e,\perp}\big)(\hat{\mathbf{u}}\cdot\hat{\mathbf{n}})^2\big)\Big) \quad (2)$$

In this study fiber bundles are not assumed to be parallel (as in (Fieremans et al., 2011)) but rotationally symmetric. Therefore, fODF follows the Watson distribution $\mathcal{P}(\hat{\mathbf{u}}) \propto \exp\Big(\kappa(\hat{\mathbf{u}}\cdot\hat{\mathbf{c}})^2\Big)$, where κ is the concentration parameter and $\hat{\mathbf{c}}$ is the symmetry axis. This model was chosen due to the fact that its axial symmetry assumption is valid for majority of spinal cord (SC) WM. In addition, it has a high range of validity, and is analytically related to DKI parameters (Jespersen et al., 2017; Novikov et al., 2018b).

For this study, the WMM parameters chosen to be assessed were those sensitive to neural damage (Falangola et al., 2014; Kelm et al., 2016); in particular, f, a biomarker for axonal loss (Fieremans et al., 2012) linked to myelin content and axon density (Kelm et al., 2016), D_a, which is associated with intra-axonal injury (Hui et al., 2012), $D_{e,\perp}$ which through tortuosity is related to the g-ratio (Jelescu et al., 2016) and $D_{e,\parallel}$ which is a marker of

demyelination (Fieremans et al., 2012). In addition, a measure (Grussu et al., 2017) of fiber dispersion κ was studied.

For this study, DKI data was used as a starting point for WMM parameters estimation. This approach is commonly used in different models of tissue microstructure (Fieremans et al., 2011; Hansen et al., 2017; Hui et al., 2015; Jespersen et al., 2012; Novikov et al., 2018b; Novikov and Kiselev, 2010; Szczepankiewicz et al., 2016). Fitting DKI instead of straightforward fit of WMM parameters, enables usage of linear least squares algorithms that yield stable estimates (Chuhutin et al., 2017) decreasing the chances to end up in a local minimum. WMM fit at order b^2 yields two solutions that fit data equally well (Novikov et al., 2018b). Using DKI fit and consequently estimating the WMM parameters allows to choose a particular solution branch (Jelescu et al., 2015b) explicitly.

2.2. Animal treatment

Female C57BL/6j bom (B6) mice aged 6–8 weeks obtained from Taconic Europe A/S, (Lille Skensved, Denmark) were maintained in the Biomedical Laboratory, University of Southern Denmark (Odense).

Mice were immunized at age of 8–10 weeks by injecting subcutaneously 100μl of an emulsion containing 100μg myelin oligodendrocyte glycoprotein $(MOG)_{p35–55}$ (TAG Copenhagen A/S, Frederiksberg, Denmark) in incomplete Freund's adjuvant (DIFCO, Alberstslund, Denmark) supplemented with 400 μg H37Ra *Mycobacterium tuberculosis* (DIFCO). Bordetella pertussis toxin (300 ng; Sigma-Aldrich, Brøndby, Denmark) in 200 μl of phosphate buffered saline (PBS) was injected intraperitoneally at day 0 and day 2. Animals were monitored daily from day 5 and scored as follows: 1, loss of tonus of up to half of the tail; 1.5, loss of tonus of more than half of the tail; 2, complete loss of tail tonus; 2.5, difficulty in walking (one leg); 3, Difficulty walking (both legs); 3.5, paresis in one hind leg; 4, paresis both hind legs; 4.5, paralysis of one hind leg; 5, paralysis of both hind legs. About 75% of the mice showed symptoms of EAE. All the scoring was performed by the same person (AW) with previous experience of EAE animal assessment (Wlodarczyk et al., 2014). Severe EAE usually developed 14–18 days after immunization. Based on the provided EAE-scale, the animals were divided into roughly equisized groups of samples: low-grade (EAE score 1.5–2, 5 samples), intermediate (2.5–4, 3 samples), high (4.5–5, 5 samples). If not stated otherwise, the control group (non-manipulated age matched animals) is henceforth referred to as zero-grade for convenience (5 samples).

Animal experiments were approved by Danish Animal Experiments Inspectorate (approval number 2014–15-0201–00369).

2.3. Sample preparation

Mice were euthanized by pentobarbytol overdose and transcardially perfused with PBS followed by 4% buffered paraformaldehyde (PFA) (pH 7.4). The spinal column was extracted and stored in 4% PFA for 7 days. On day 8, now fully fixed cords were manually dissected out of spinal column, and stored in 4% PFA with the meninges removed until MRI. 24 hours prior to the experiment, the samples were washed in PBS to remove PFA and to minimize associated T_2*-related signal attenuation (Shepherd et al., 2009, 2005). The

SC was cut into 3 parts and segments from T8 up to L6 were selected for imaging. We differentiate between three segments of mouse SC as follows: mid-thoracic (MTO):T8-T11, lower thoracic (LTO):T12-LU1, lumbar (LU):L2-L6.

2.4. MR imaging

Imaging was performed on a 16.4 T vertical bore Bruker Biospin (Ettlingen, Germany) Aeon Ascend magnet equipped with a Micro5 probe and a gradient unit capable of delivering up to 3000 mT/m in all directions. The samples were placed in a 5 mm NMR tube filled with Fluorinert© 3M and held parallel to the direction of the main magnetic field using a polypropylene straw. The temperature was monitored and maintained at 23.6°C using air flow.

In order to increase the prospective impact of the study we used a variant of standard Stejskal-Tanner pulse sequence that is commonly implemented in human scanners. Thus, diffusion kurtosis data were acquired using a 2D diffusion weighted fast spin echo sequence with echo train length (ETL=8), first echo time (effective echo time (TE) = 15 ms), echo spacing (ESP=4.23 ms), total repetition time (TR=2000ms)(Beaulieu et al., 1993; Kelm et al., 2016; West et al., 2018). Receiver bandwidth (BW) for signal acquisition = 83 kHz. For each SC, between 16 and 22 0.5mm-thick slices were scanned. For each slice, a matrix of size 120 × 120 voxels with field of view (FOV) (FOV=4.2 mm × 4.2 mm) (resolution of 0.035 mm × 0.035 mm) was acquired. Diffusion weighting was performed with short gradient pulses of duration (δ=1.5ms) and separation (diffusion time) Δ = 10ms. Diffusion weighting with b-values of 0.2,0.3,0.5,0.6,0.9,1,1.2,1.5,1.8,2.1,2.5 ms/μm^2 was applied along 30 directions, with 1 average (NA) for b < 1.2 ms/μm^2 and 2 averages for b > 1.2 ms/μm^2. Sixty b = 0 ms/μm^2 images were collected for normalization. The total scanning time per spinal cord was about 10 h. Examples of images acquired with b = 0.2ms/μm^2 are provided in Fig. 1 (A,B). SNR (amplitude ratio) of the acquired raw data was estimated to be ~30–40 (in WM, b = 0), ~50 (in GM, b = 0), ~30 (in WM, $b = b_{max}$), ~20 (in GM, $b = b_{max}$).

High resolution T_2*-weighted images for lesion delineation were acquired using fast low angle shot (FLASH) pulse sequence with twice the in-plane resolution (0.018 mm × 0.018 mm) and the same slice thickness (0.5 mm), NA = 2 and TE = 5ms.

2.5. Image segmentation

Image segmentation of white and gray matter was performed manually based on the mouse spinal cord atlas (Watson, 2009).

Lesions were manually outlined on T_2*-weighted slices as described in (Steinbrecher et al., 2005) and thereafter lesion contours were downsampled to the resolution of DWI maps. On each slice, potential abnormalities were inspected and compared to the atlas. Voxels with abnormal hyperintensity that could not be explained by the anatomical features of SC, were manually marked using an in-house developed software tool. Delineation followed a conservative definition of the lesion. As such, whenever there was a suspicion that the increase in WM intensity could be explained by anatomical features, the voxels were not delineated as lesion. The slices and spinal cords were presented in randomized order and the examiner (AC) was blinded to the grade. An example of this segmentation is shown in Fig.

2. NAWM was defined after the segmentation as a non-lesion WM. Lesion load was defined as fraction of volume taken by abnormal hyperintensity in T_2*-weighted images.

2.6. Parameter estimation

The raw images were denoised using the Marchenko-Pastur PCA method (Veraart et al., 2015) and subsequently corrected for Gibbs ringing artefacts (Kellner et al., 2015) before further analyses. Standard single diffusion encoding technique that was used in this study is capable of accessing only fully symmetric diffusion and kurtosis tensors. Therefore, twenty-two independent components of fully symmetric diffusion and kurtosis tensors (Jensen et al., 2005) were fit to the data using interior-point weighted linear least squares algorithm (Veraart et al., 2013) implemented in Matlab. Based on (Chuhutin et al., 2017), WM voxels were fit up to a maximum b-value of $b_{\max} = 2.5$ ms/μm^2, and GM voxels were fit up to $b_{\max} = 1.2$ ms/μm^2. The fit quality was inspected for each sample. An example of data fit for a representative voxel in WM lesion, NAWM and GM is shown in Fig. 1 (C,D). Diffusion and kurtosis tensor parameters were calculated according to (Hansen et al., 2014, 2013; Jensen et al., 2005; Jensen and Helpern, 2010). The exact analytical derivations of WMM parameters from the elements of diffusion and kurtosis tensors used in this study are provided in (Jespersen et al., 2017) (assuming a Watson distribution of neurites). The general case is presented in (Novikov et al., 2018b). Different sets of WMM parameters can yield the same DKI signal, an effect known as parameter degeneracy, and a subject of current interest (Jelescu et al., 2015a, 2015b). However, in this work, only parameters corresponding to the so-called ‘plus’ branch (Hansen and Jespersen, 2017; Jespersen et al., 2017; Novikov et al., 2016), typically having $D_a > D_{e,\parallel}$ were considered. This choice was guided by the recent publications (Kunz et al., 2018), that suggest ‘plus’ branch solution to be biologically plausible. Less than 10% of voxels in any slice displayed non-physical values, such as a negative diffusivity. These voxels were excluded from further statistical analysis of WMM parameters. In total, for all spinal cords, 245851 GM voxels and 246393 WM voxels were analyzed for DTI/DKI parameter estimation, while WMM parameters were estimated in 232274 voxels.

In WM, the estimated parameters were: axial diffusivity ($D_\parallel$), radial diffusivity ($D_\perp$), fractional anisotropy (FA), axial kurtosis ($K_\parallel$), radial kurtosis ($K_\perp$), which were included for a model independent assessment and the previously mentioned WMM parameters (extra-axonal radial $D_{e,\perp}$ and axial $D_{e,\parallel}$ diffusivities, intra-axonal diffusivity D_a, volume fraction of axonal compartment f, and concentration parameter of the Watson distribution, κ). In GM the low tissue anisotropy causes the estimated direction of primary eigenvector to be unstable/poorly defined, and thus, the values of axial and radial diffusivity and kurtosis are less reliable/meaningful. Due to that and in order to restrict the number of compared parameters to avoid unnecessary multiple comparisons, it was decided to limit the scope of estimated parameters in GM to MD and MKT.

2.7. Statistical Analysis

The voxels from all spinal cords were input to a linear mixed effects model (LME) (Gelman and Hill, 2007; Goldstein, 2011).

The choice of model was guided by current recommendations in (Barr et al., 2013; Bolker et al., 2009) and iterative maximization of Akaike information coefficient (Akaike, 1998).

The choice of LME to estimate and study the effects of EAE on kurtosis tensor parameters was guided by the observations that pathological changes both inside lesions, in NAWM and in GM contribute to clinical disability in both human MS and in animal models of neurodegeneration (de Kouchkovsky et al., 2016; Evangelou et al., 2000; Filippi et al., 2012; Filippi and Rocca, 2011; Inglese and Bester, 2010; Kipp et al., 2016; Lassmann and Bradl, 2016). The specific form of the LME designed to take into account random contributions of sample to sample variability. Our assessment of LME fitting quality (in Table 2) was in line with up-to-date recommendations for LME (Baayen et al., 2008; Edwards et al., 2008; Nakagawa et al., 2013).

Each of 12 examined parameters p_i was thus fit to

$$p_i \sim g \cdot s + l + (g \cdot s \,|\, a) + (l \,|\, a) \tag{3}$$

using Wilkinson notation (Wilkinson and Rogers, 1973), where g is grade, s is slice, lesion is l, a is sample (animal)[1]. The 'fixed' effects part of the model was designed to allow the parameters to depend on grade, while the size of the effect was permitted to be different in various SC segments (first term). The second term encodes the expected difference in parameter values inside ($l = 0$) and outside ($l = 1$) the T_2* hyperintense lesions. Sample-to-sample variations were allowed by including 'random' effects for segment, grade and lesion, each grouped sample-wise.

To avoid a small number of data points having an undue influence on the regression, outliers 2.5 standard deviations above and below the model residual means were removed after the initial fit, and the model was refitted. This procedure is in agreement with literature (Baayen, 2008; Baayen et al., 2008; Tremblay and Tucker, 2011). By verifying that predictors are significant before and after the outlier removal we verified that the extreme values do not substantially influence the regression. The removed outliers constitute less than 4% of data. The comparison of in outliers and the rest of the data in terms of quality of fit (χ^2) is given in Supplementary material.

For each of the 'fixed' effects, analysis of variance (ANOVA) p-values were calculated. These p-values represent the significance of individual fixed effects as well as the combined effect of segment and grade on parameter. The p-values describing the significance of the linear relationship between the measured parameter and the grade of disability of the EAE animal were finally reevaluated using the false discovery rate (FDR) procedure (Benjamini and Hochberg, 1995).

The quality of the fit of LME was estimated using R^2_β (Edwards et al., 2008), so that

[1]The notation (l|a) stands for a random effect of lesion (l) being grouped by sample (a). The notation $g{\cdot}s$ stands for an effect of grade (g), slice (s) and a combination of these two ($g{\cdot}s = g + s + g{:}s$).

$$R^2_{\beta} = \frac{(q-1)\nu^{-1}F\left(\hat{\boldsymbol{\beta}}, \hat{\Sigma}\right)}{1+(q-1)\nu^{-1}F\left(\hat{\boldsymbol{\beta}}, \hat{\Sigma}\right)} \quad (4)$$

where $F\left(\hat{\boldsymbol{\beta}}, \hat{\Sigma}\right)$ is a statistic corresponding to the null hypothesis H_0: $\beta_1 = \beta_2 = \ldots = \beta_{q-1} = 0$ for $q-1$ fixed effects, β_i, ν is Satterthwaithe's estimate of effective degrees of freedom. Partial $R^2_{\beta}\left(R^2_{\beta,\,p}\right)$ were calculated to obtain the relative measure for each of the 'fixed' effects that corresponds to the null hypothesis $H_0 : \beta_j = 0$ for $j \in \{1,\ldots,\, q-1\}$.

While the LME analysis was performed primarily to discern which DKI/WMM parameters correlate with disability and which tissues are affected, a following post-hoc analysis aimed to check the sensitivity of the chosen parameters. The parameter means were calculated for each sample, for each SC segment, and for the SC as a whole, in GM and WM separately. The parameters surviving FDR correction of LME p-values were checked and the grades with significantly different means were identified using two sample tests (one-way ANOVA, followed by FDR correction). For the post-hoc analysis, no outlier removal was performed.

A further post-hoc comparison of individual parameters inside lesions supported the initial LME model assumption of independence between the grade and lesion LME model parameters (data not provided). Thus, we based the post-hoc lesion analysis on the premise that the distribution of parameters inside lesions does not depend on segment or EAE grade.

Quantitative results (mean and standard deviation along the disability group, no outlier removal) for all the measured parameters are provided in Table 1. The most distinct changes are observed in GM MKT and NAWM $K\perp$ (decrease) and an increase in $D_{e,\parallel}$ in NAWM. Of all the measured parameters $D_{e,\parallel}$ has the highest variance.

3. Results

3.1. Diffusion MRI: Parameter estimation

A one-way-ANOVA of sample-wise mean of relative lesion load showed that controls were significantly different from the diseased (EAE) animals in all segments (provided in Supplementary material). However, despite apparent increase in the mean values of lesion load, the variance of lesion load increases in SC slices of high grade animals. Subsequently, the lesion load is unable to statistically significantly discriminate between grades of disability.

Figure 3 shows maps of all the investigated parameters for a representative animal in each of the grades (control, low, intermediate, and high grade) in the medium thoracic (T9) segment. WMM parameters are restricted to the manually delineated WM to approximately fulfill the assumptions of the model. Qualitatively, the maps show an increase in asymmetry in animals with higher disability grade. The Watson concentration parameter κ displays the biggest variation in the maps. Parameters that are accessible with DTI (apart from MD) show better contrast between WM and GM. However, parameters derived from DKI and WMM show more variability inside WM.

3.2. Diffusion MRI: validating metrics with LME

Table 2 shows the estimators of the LME fit quality and values that quantify the capability of LME model parameters to explain each of the parameters.

All parameters demonstrated relatively good quality of fit $R^2_{\tilde{\beta}}$. MD and $D_{e,/\!/}$ attained the lowest values of ~0.91.

P-values shown in Table 2 quantify the extent to which each of the 12 studied parameters can be explained by the parameters of the linear mixed effects model. Grade had a significant effect on 7 out of 12 parameters after FDR: MKT in GM, and $K\perp$, $D\perp$, $D_{e,/\!/}$, $D_{e,\perp}$, κ and f in WM. All parameters except MD and MKT in GM and f in WM were found to depend significantly on the segment. Likewise, the interaction between grade and segment was statistically significant in all but five parameters, i.e. the two GM parameters MD and MKT, three WM parameters $D_{e,/\!/}$, D_a and $D_{/\!/}$. All parameters but D_a were significantly different between lesion and normal appearing brain tissue.

The results of the calculation of partial $R^2_{\tilde{\beta},p}$ (Edwards et al., 2008) for each fixed effect variable are also provided in Table 2. $R^2_{\tilde{\beta}}$ revealed high association between the kurtosis/WMM parameters and the disability grade of EAE (~0.9) for all the parameters that were found significant in FDR procedure. The comparison of $R^2_{\tilde{\beta},p}$ values showed that the disability grade accounted for most of the variation in 4 out of 12 parameters $D\perp$, $D_{e,\parallel}$, $D_{e,\perp}$ in WM and MKT in GM.

Additional characteristics of the LME fit are provided as Supplementary material. These include a different measure of fit quality (Johnson, 2014; Nakagawa et al., 2013) and estimates and confidence intervals of fixed effects of LME-model. These estimates show that among the parameters which are significantly correlated with the grade, MKT, $K\perp$, f, $D_{e,\perp}$ and κ decrease with the increase in disability grade, while $D\perp$ and $D_{e,\parallel}$ increase with increasing grade. The LME results have the same direction and magnitude of decrease or increase as overall means in Table 1.

3.3. Diffusion MRI: Post-hoc statistical analysis

From the LME analysis, we found that the variation of several GM and WM parameters can be explained by EAE-grade and by lesion status, i.e. whether or not the voxel is located inside a lesion. A follow-up post-hoc analysis intended to investigate group-wise behavior of the segment-wise means in parameters with a significant grade. In particular, Table 3 shows the results of the post-hoc analysis of sample means outside the lesions, in GM and NAWM.

In GM, MKT showed significant difference between the grades only in the slices located in mid-thoracic segment of the spinal cord, specifically between low and intermediate and between low and high grades.

In NAWM, 5 out of the 6 biomarkers surviving FDR correction demonstrated significant differences between the control and diseased animals, mainly in the lumbar SC. Two DKI parameters ($K\perp$, $D\perp$), and two WMM parameters (f, $D_{e,\parallel}$) depended significantly on EAE

grade. $K_\perp$ and f were found to survive pooling all segments together, demonstrating an overall significant difference between high and low grade.

As an illustration, a representative part of the data and the associated post-hoc analysis is given in Fig. 4. In this figure, the distributions over voxels of MKT in GM (Fig. 4 (A)) and $K_\perp$ in NAWM (Fig. 4 (B)) are visualized using box plots for each of the grades and segments. The means of each of the spinal cords, which were used in the post-hoc analysis (Table 3), are superimposed on the boxplots as blue circles. The significantly different grades are marked by asterisks. Note that the seemingly large number of outliers apparent in the box-plots of Fig. 4 constitute a small fraction of the more than 10000 voxels sampled for each spinal cord.

The same type of post-hoc analysis that was used to study the voxels outside of the lesions, was used to investigate voxels inside the lesions. The analysis revealed that the vast majority of segment-wise means inside the hyperintensity lesions did not show any significant differences between EAE-grades, with only $K_\parallel$ in lower thoracic segment showing difference between the grades at the level of significance $p < 0.05$ (results of this analysis are provided as Supplementary material).

The results of an additional post-hoc analysis adapted to test for difference in parameter means between lesions and NAWM, revealed that the difference is significant for all 10 WM parameters are provided in Supplementary material.

3.4. Combining T_2*-weighted images and diffusion MRI

Based on the presented results, that report lesion load to be insignificantly related to disability grade, we next consider a “hybrid” way of addressing the lesion load and DKI parameters. It can be done e.g. using a compound variable that reflects both lesion load and NAWM health to provide a way of distinguishing different grades of EAE. In particular, an animal-wise LME fit of the model

$$g = p_0 + p_1 \cdot l + p_2 \cdot \widehat{K}_\perp + p_3 \cdot \widehat{D}_{\mathrm{e},\,\parallel} \tag{5}$$

where g is the grade and l is lesion load, $\widehat{D}_{\mathrm{e},\,\parallel}$ and $\widehat{K}_\perp$ are animal-wise mean values of $D_{\mathrm{e},\parallel}$ and $K_\perp$ in NAWM, yielded coefficient values $p_0 = 2.9$, $p_1 = 12.7$, $p_2 = -2.3$, $p_3 = 10.4$ ms/μm^2. A “hybrid” metric that uses these parameters is able to distinguish not just between control and high, control and intermediate groups but also between low and high, low and intermediate EAE-grades. The results of using such metric are shown in Fig. 5. However, a follow up study that will test this hybrid metric with an independent data is needed.

4. Discussion

Mapping quantitative biomarkers in MS – as well as in other neurological disorders – is essential for early diagnosis, follow up of treatments, and testing novel avenues for treating disease. Lesion load is a biomarker that is easily and commonly imaged both in humans and in preclinical studies. However, even though it has been historically associated with motor deficits in MS and EAE (Bjartmar et al., 2001; Sathornsumetee et al., 2000), its

correlation with disability is poor (Barkhof, 2002; Bergers et al., 2002; Robinson et al., 2010; Wuerfel et al., 2007), a disparity known as the clinico-radiological paradox (Cohen et al., 2016; Nathoo et al., 2014). Confirming the clinico-radiological paradox in MS and previously published results in EAE (Wuerfel et al., 2007), we did not find correlations between the EAE-grades and lesion load. In addition, using DKI provided no obvious advantages for structural segmentation. We therefore turned to LME fitting of the metrics that map microstructural aspects of the tissue. Instead of trying to improve on lesion load detection, the study aimed to test additional quantitative metrics obtained from DKI against disease severity in an animal model of MS.

In GM, MKT depended significantly on disability grade (Tables 2 and 3; Fig. 4). This is in line with human studies (Agosta et al., 2007; Bester et al., 2015; Raz et al., 2013; Zackowski et al., 2009) reporting similar changes in GM. Such changes are likely indications of GM pathology, possibly associated with neuronal degeneration and myelin loss (Guglielmetti et al., 2016). Interestingly, while the biggest burden of lesions and most of the changes in NAWM (Table 3; Fig. 4) were associated with the lumbar section of the spinal cord, most of the changes detected in GM were observed in mid-thoracic sections. Given that the EAE-induced disability progresses from hind- to forelimbs, one might hypothesize that the damaged GM tissue in mid thoracic SC is connected to the damaged fascicles in lumbar WM. Thus, in EAE, correlated pathological mechanisms may be responsible for damage in NAWM and GM. This may be similar to human MS, where the spatial and temporal relationships between the damage in GM and NAWM are still not fully resolved and might depend on disease phenotype (Bodini et al., 2009; Pirko et al., 2007; Steenwijk et al., 2015; Tewarie et al., 2018).

In NAWM, $K\perp$ and $D\perp$ showed the strongest and most robust results among tissue biomarkers derived from kurtosis and diffusion tensors. Radial kurtosis showed the strongest inverse relationship with EAE grade (i.e. it decreased with increasing disease severity). Such changes have also been observed previously in preclinical models of MS (Falangola et al., 2014; Jelescu et al., 2016; Kelm et al., 2016), while the opposite effect was observed in (Guglielmetti et al., 2016). This agreement might suggest closer similarities of the EAE to cuprizone or genetically induced chronic demyelination than to the acute inflammatory demyelination used in (Guglielmetti et al., 2016). An increase in $D\perp$ was also found to be significantly correlated with EAE grade. Again, this behavior agrees with previous chronic demyelination studies (Falangola et al., 2014; Jelescu et al., 2016; Kelm et al., 2016) and with results of a previous DTI EAE study (Budde et al., 2009). Early human studies demonstrated similar behavior of $D\perp$ and associated it with demyelination (Klawiter et al., 2011) and possible axonal loss (Naismith et al., 2010).

Among WM model parameters, $D_{e,\parallel}$ was the one affected the most by EAE grade, while $D_{e,\perp}$ was affected in a much weaker manner and with no significant effects in post-hoc analysis (Tables 2 and 3). Counter-intuitively, an increase in $D_{e,\parallel}$ with grade was found. This fact could potentially be explained by axonal damage, changes in the structure of glial cells, and myelin loss, causing the extra-axonal space to have higher diffusivity. This result is in contrast with cuprizone models (Falangola et al., 2014; Guglielmetti et al., 2016; Jelescu et al., 2015b). The disparity can stem from differences between the mechanisms underlying

tissue degeneration but also from other microstructural differences between the neural tissue in cerebrum and in spinal cord. Alternatively, it may also be a result of choosing a different solution ‘branch’ when finding parameters of WMM model (Hansen et al., 2017; Jelescu et al., 2015b; Jespersen et al., 2017).

The axonal water fraction (previously suggested to be a biomarker of axonal loss (Fieremans et al., 2011)) was also significantly affected by the differences in EAE grade. We found f to decrease with an increase in EAE-grade, therefore an axonal loss in NAWM could be one driver of the disability.

The ratio $\lambda = D_{e,\parallel}/D_{e,\perp}$ (tortuosity) has been proposed as a biomarker of demyelination (Fieremans et al., 2012). In our data (see Results and Supplementary material), $D_{e,\parallel}$ increased strongly and $D_{e,\perp}$ decreased, thus overall tortuosity increased with increase in grade (the effect of grade on tortuosity variation was found to be significant in post-hoc LME fit, data available upon request). This finding is in contrast to (de Kouchkovsky et al., 2016; Falangola et al., 2014) and may provide evidence of pathological processes in EAE.

Our data shows that the Watson concentration parameter κ significantly decreased in a way that could be explained by EAE grade. This might be a result of axonal damage that could cause the breaking of fascicles and fanning out of individual axons. According to post-hoc analysis, this behavior was present in the lumbar segment of the spinal cord. Our result is in line with (Schneider et al., 2017), where increased fiber dispersion in NAWM of MS SC was reported. However, in our study increased fiber dispersion is present inside the lesions in mouse SC as well. This is in contrast with (Grussu et al., 2017), where a decrease in neurite orientation dispersion was measured in lesions of MS using neurite orientation dispersion and density imaging (NODDI) and histology. One possible reason for the disparity is different species (animal and human), where different pathological mechanisms could be at play. Another reason could be related to focal lesions being not as well defined in rodent models, and in EAE in particular, as in humans. Therefore, even though lesion detection was performed in a consistent and ‘blind’ way, a systematic error may have been introduced, e.g. if too big portions of NAWM are segmented as lesions. Third, differences in the employed diffusion models could be responsible for the disparity. This discrepancy may be addressed by validation of fiber dispersion in EAE and MS lesions using microscopy.

$D_{\parallel}$ has previously been shown to decrease significantly with EAE score and with axonal injury (Budde et al., 2009). Both $K_{\parallel}$ and $D_{\parallel}$ were significantly affected in some cuprizone studies (Falangola et al., 2014; Guglielmetti et al., 2016) but not in (Jelescu et al., 2016; Kelm et al., 2016). Our study found no evidence of any correlation between EAE grade and $D_{\parallel}$ or $K_{\parallel}$. Consequently, our work provides an indication that in EAE, tissue changes due to demyelination and axonal loss are insufficient to change diffusivity or kurtosis parallel to fiber bundles.

In our study, FA showed no significant dependence on grade. This observation is in line with (Guglielmetti et al., 2016) where FA was not able to differentiate between the treatment groups and control.

Both the results of LME model fitting and post-hoc analysis demonstrated that all parameters but one (D_a) were able to distinguish lesions from NAWM. Together with that, in a more intriguing finding of this work the vast majority of the biomarkers measured within lesions did not differ across grades. A probable explanation of that is that there is no detectable differences in lesion microstructure between the grades. This may be evidence that CNS tissue that makes up WM lesions does not contribute to disability in EAE.

Recent studies (By et al., 2018, 2017; Grussu et al., 2015; Schneider et al., 2017) have applied NODDI and spherical means (SMT) techniques to spinal cord tissue WM in healthy controls and in MS patients and demonstrated promising diagnostic results. However, our findings suggest that the basic assumptions of these studies may not be fulfilled in all cases. In particular, since D_a was found not to be driven by EAE grade while $D_{e,\parallel}$ increased with grade, those two parameters cannot be constant as assumed in NODDI ($D_a = D_{e,\parallel} = 1.7\mu m^2/ms$). The constant tortuosity assumption (imposed in both NODDI and SMT) was also not valid in our dataset. Thus, assuming that our results are valid in human MS, the values estimated with those two techniques would be unable to reveal the true microstructural changes associated with disease progression and disability. Thus, it may prove necessary to allow all the parameters of the so-called ‘standard’ model (Novikov et al., 2018b; Jelescu et al., 2015a; Jespersen et al., 2007) to be determined by the fit.

5. Limitations

In this work, fixed tissue was used, which allowed longer scanning and better data quality (e.g due to motion and susceptibility effects of vertebrae) in comparison with in vivo protocols. This choice was justified by the assumption that despite known impact of fixation on tissue properties (Shepherd et al., 2009, 2005; Sun et al., 2005) the pathological effect on damaged tissue will be strong enough to be detectable in the present exploration study. Nonetheless, the results of this study are influenced by differences between ex-vivo and in-vivo tissues, which have not been fully accounted for yet (Horowitz et al., 2015).

Manual lesion segmentation, even though it was performed ‘blindly’, can potentially result in a systematic bias in contrast between estimated NAWM and lesion values, as well as increased variability.

Concerns have been expressed (Lampinen et al., 2018) about applicability of modeling constraints required for multi-compartmental modeling of diffusion in neural tissue. The compartment models for diffusion used in this work have not been fully validated across different tissue types, in vivo and ex vivo datasets, etc. However, in this study the modeling efforts were restricted to ex-vivo mouse spinal cord, where, according to histology (Ong et al., 2008) the axonal size is around 1μm and in the chosen regime of gradient strengths and waveforms the attenuation due to diffusion along the diameter is negligible (Dyrby et al., 2013; Nilsson et al., 2017). Chosen diffusion times are short enough (10ms), so that the exchange has only a minimal effect (Nilsson et al., 2013, 2009). Therefore, there is good reason to believe that in this case, the approximation of axons as sticks is approximately valid. Further investigation of the validity of the attained results e.g. the role of myelin water

and related compartment-dependent T_2-relaxation of diffusion weighted signal is necessary before translating the results of this study to the clinic.

6. Clinical implications

This work shows that the disability in EAE and therefore probably also disability in MS is correlated with and maybe is even driven by the neural matter outside the lesions.

In line with other works, this study also suggests the prominent role of SC GM (Agosta et al., 2007; Bester et al., 2015; Guglielmetti et al., 2016; Raz et al., 2013; Zackowski et al., 2009) and NAWM (Falangola et al., 2014; Jelescu et al., 2016; Kelm et al., 2016) in the development of disability. All these results support the fact that the search for disability biomarkers in human SC should concentrate on the neural matter outside the WM lesions. Future longitudinal studies could elucidate whether GM damage is a precursor of damage in NAWM.

This study was performed with 11 *b*-values and 30 directions, yielding approximately 350 images. However, such a big number of *b*-values was primarily needed to estimate parameters in different tissues. If a similar approach would be used but focussed e.g. only on the WM, the same type of analysis can be performed with 5 *b*-values and 30 directions, which can be achieved within a clinically feasible scan time of around 15 minutes. At the same time, due to relatively low *b*-values, this protocol is more accessible for clinical systems than two compartment models such as CHARMED (Assaf et al., 2004; Assaf and Basser, 2005; Barazany et al., 2009; De Santis et al., 2016) developed to attempt axonal diameter mapping.

This study points on the perspective of using WMM, where extracellular parallel diffusivity and axonal water fraction are recommended for assessment of human MS disability using SC MRI. Parameters of the full WMM in human MS spinal cord can be estimated and compared to our results along with other animal models (e.g. progressive model as in (Al-Izki et al., 2012)). Comparing between the biomarkers in different models can help to reassess models of spinal cord pathology in MS. Since the damage in spinal cord is better correlated with accrual of long-term disability (Inglese and Bester, 2010; Lin et al., 2006) than damage in cerebrum, the results of such an assessment can improve the understanding of mechanisms of MS progression.

There are some barriers in translation of the results of this work to a clinical setting. In addition to human MS pathology being distinct from the EAE animal model in terms of illness onset and its progression, human scanners feature multiple technical differences compared to the system used here. Such differences pose some challenges in the adaptation of the described methods.

In particular, this study has been performed with an ultra-high magnetic field strength. On clinical systems with much lower magnetic field, the relaxation times are different. Since myelination and compartmental relaxation significantly influence the parameters of microstructural model (Lampinen et al., 2019), the magnitude of the effect of disability on WMM parameters may be altered. In addition, robust determination of model parameters, is

not straightforward on clinical scanners in vivo, mainly due to gradient strength limitations, and this is an active area of research. Current promising paths involve acquisition of "orthogonal information" that constrains parameter estimation. Such information can be provided by unconventional diffusion sequences e.g. Double Diffusion Encoding (Coelho et al., 2019; Reisert et al., 2019). Until the effect size of disability on our white matter model has been investigated on clinical systems, we recommend to use the DKI-parameters: $K_{\perp}$, $D_{\perp}$ in NAWM and MKT in GM.

An additional obstacle in translation of the presented results to clinical setting is due to motion artefacts and susceptibility effects of vertebrae. The state-of-the-art method (Wheeler-Kingshott et al., 2014) to mitigate these is using cardiac triggering and careful shimming by e.g dedicated spinal cord shimming coils (Topfer et al., 2016). Recent studies (By et al., 2018, 2017; Hori et al., 2014; Li and Wang, 2017; Raz et al., 2013), which were designed based on these recommendations, succeeded to estimate DKI biomarkers in human cervical spinal cord. In addition to that, dedicated acquisition methods (Hansen et al., 2016) can speed up the acquisition of DKI metrics (such as MKT in GM and $K_{\perp}$ in NAWM) that were found sensitive in this study.

Overall the DKI data as acquired in human scanners has lower SNR and is more artefact-prone than in preclinical ex vivo setup, and therefore there are still considerable issues to be solved before applying these methods on the MS patients. However, the high significance of changes presented in this study suggests that with adoption of new methods, these results will be relevant for clinical use.

7. Conclusions

- In NAWM and GM the relationship between the disability and DKI and DTI metrics was found to be similar to other hypomyelinating MS models and to ex-vivo MS tissue.
- In NAWM, changes in WM-modeling parameters (strong increase in $D_{e,\parallel}$, weak effect in D_a, $D_{e,\perp}$) were clearly different to what has been observed in other animal models of MS.
- The statistical analysis based on linear mixed effect models disentangled NAWM and lesion effects. Neither accumulated lesion load, nor DWI biomarkers in the tissue restricted by T_2*-weighted lesion show any significant effect of lesions on EAE-grades.
- A strong increase in $D_{e,\parallel}$ of NAWM is an effect that has not been previously observed in other models of MS.

8. Summary

Overall, this study detects significant alterations in NAWM and GM (but not in WM lesions) in SC of EAE animals that correlate with dysfunction. These alterations are best detected with DKI and WMM biomarkers.

Supplementary Material

Refer to Web version on PubMed Central for supplementary material.

Acknowledgements

The authors are grateful for financial support of this project by Lundbeck Foundation Grant R83-A7548 and Simon Fougner Hartmanns Familiefond. AC and BH acknowledge support from NIH1R01EB012874-01.

The authors thank Dr Kevin D Harkins, and Prof. Mark D Does from Vanderbilt University for the REMMI pulse sequence and reconstruction toolbox used in this study, which were supported through grant number NIH EB019980. NS was supported in part by the European Research Council (ERC) under the European Union's Horizon 2020 research and innovation programme (grant agreement No. 679058 – DIRECT-fMRI).

The authors also thank Dina Arengoth and Pia Nyborg Nielsen for expert technical assistance. AW and TO acknowledge financial support from Lundbeck Foundation, Danish Multiple Sclerosis Society, Independent Research Fund Denmark.

The authors would also like to offer special thanks to Shemesh Lab members in Champalimaud Center for Unknown that provided their extensive help during the acquisition stages and, in particular, to Teresa Serrades Duarte, Daniel Nunes, Rui Simões and Cristina Chavarrías.

Abbreviations

$\mathbf{D_a}$	intra-axonal diffusivity
$D_\perp$	radial diffusivity
$D_\parallel$	axial diffusivity
$K_\perp$	radial kurtosis
$D_{e,\parallel}$	extra-axonal axial diffusivity
κ	concentration parameter of the Watson distribution
$K_\parallel$	axial kurtosis
$D_{e,\perp}$	extra-axonal radial diffusivity
f	volume fraction of axonal compartment
ANOVA	analysis of variance
BW	receiver bandwidth
CNS	central nervous system
DKI	diffusion kurtosis imaging
DTI	diffusion tensor imaging
DWI	diffusion weighted imaging
EAE	experimental autoimmune encephalomyelitis
ESP	echo spacing

FA	fractional anisotropy
FDR	false discovery rate
fODF	fiber orientation distribution function
FOV	field of view
GM	gray matter
LME	linear mixed effects modeling
LTO	lower thoracic segment
LU	lumbar segment
MD	mean diffusivity
MKT	mean of the kurtosis tensor
MRI	magnetic resonance imaging
MS	multiple sclerosis
MTO	mid thoracic segment
NA	number of averages
NAWM	normal appearing white matter
NODDI	neurite orientation dispersion and density imaging
PBS	phosphate buffered saline
PFA	paraformaldehyde
SC	spinal cord
SMT	spherical means technique
TE	echo time
TR	repetition time
WM	white matter
WMM	white matter model

References

Bjartmar C, Kidd G, Mörk Sverre, Rudick Richard, Trapp Bruce D., 2001. Neurological disability correlates with spinal cord axonal loss and reduced N-acetyl aspartate in chronic multiple sclerosis patients. Annals of Neurology 48, 893–901. 10.1002/1531-8249(200012)48:6<893::AID-ANA10>3.0.CO;2-B

Agosta F, Absinta M, Sormani MP, Ghezzi A, Bertolotto A, Montanari E, Comi G, Filippi M, 2007. In vivo assessment of cervical cord damage in MS patients: a longitudinal diffusion tensor MRI study. Brain 130, 2211–2219. 10.1093/brain/awm110 [PubMed: 17535835]

Akaike H, 1998. Information Theory and an Extension of the Maximum Likelihood Principle, in: Selected Papers of Hirotugu Akaike, Springer Series in Statistics. Springer, New York, NY, pp. 199–213. 10.1007/978-1-4612-1694-0_15

Al-Izki S, Pryce G, O'Neill JK, Butter C, Giovannoni G, Amor S, Baker D, 2012. Practical guide to the induction of relapsing progressive experimental autoimmune encephalomyelitis in the Biozzi ABH mouse. Multiple Sclerosis and Related Disorders 1, 29–38. 10.1016/j.msard.2011.09.001 [PubMed: 25876448]

Allen IV, McQuaid S, Mirakhur M, Nevin G, 2001. Pathological abnormalities in the normal-appearing white matter in multiple sclerosis. Neurol Sci 22, 141–144. 10.1007/s100720170012 [PubMed: 11603615]

Assaf Y, Basser PJ, 2005. Composite hindered and restricted model of diffusion (CHARMED) MR imaging of the human brain. NeuroImage 27, 48–58. 10.1016/j.neuroimage.2005.03.042 [PubMed: 15979342]

Assaf Y, Freidlin RZ, Rohde GK, Basser PJ, 2004. New modeling and experimental framework to characterize hindered and restricted water diffusion in brain white matter. Magn. Reson. Med 52, 965–978. 10.1002/mrm.20274 [PubMed: 15508168]

Baayen RH, 2008. Analyzing linguistic data: a practical introduction to statistics using R Cambridge University Press, Cambridge, UK; New York.

Baayen RH, Davidson DJ, Bates DM, 2008. Mixed-effects modeling with crossed random effects for subjects and items. Journal of Memory and Language, Special Issue: Emerging Data Analysis 59, 390–412. 10.1016/j.jml.2007.12.005

Baker D, Amor S, 2014. Experimental autoimmune encephalomyelitis is a good model of multiple sclerosis if used wisely. Multiple Sclerosis and Related Disorders 3, 555–564. 10.1016/j.msard.2014.05.002 [PubMed: 26265267]

Bakshi R, Thompson AJ, Rocca MA, Pelletier D, Dousset V, Barkhof F, Inglese M, Guttmann CR, Horsfield MA, Filippi M, 2008. MRI in multiple sclerosis: current status and future prospects. The Lancet Neurology 7, 615–625. 10.1016/S1474-4422(08)70137-6 [PubMed: 18565455]

Barazany D, Basser PJ, Assaf Y, 2009. In vivo measurement of axon diameter distribution in the corpus callosum of rat brain. Brain 132, 1210–1220. 10.1093/brain/awp042 [PubMed: 19403788]

Barkhof F, 2002. The clinico-radiological paradox in multiple sclerosis revisited. Current Opinion in Neurology 15, 239. [PubMed: 12045719]

Barr DJ, Levy R, Scheepers C, Tily HJ, 2013. Random effects structure for confirmatory hypothesis testing: Keep it maximal. Journal of Memory and Language 68, 255–278. 10.1016/j.jml.2012.11.001

Basser PJ, Pierpaoli C, 1996. Microstructural and Physiological Features of Tissues Elucidated by Quantitative-Diffusion-Tensor MRI. Journal of Magnetic Resonance, Series B 111, 209–219. 10.1006/jmrb.1996.0086 [PubMed: 8661285]

Beaulieu CF, Zhou X, Cofer GP, Johnson GA, 1993. Diffusion-weighted MR microscopy with fast spin-echo. Magnetic Resonance in Medicine 30, 201–206. 10.1002/mrm.1910300208 [PubMed: 8366801]

Benjamini Y, Hochberg Y, 1995. Controlling the False Discovery Rate: A Practical and Powerful Approach to Multiple Testing. Journal of the Royal Statistical Society. Series B (Methodological) 57, 289–300.

Berger JR, 2011. Functional improvement and symptom management in multiple sclerosis: clinical efficacy of current therapies. Am J Manag Care 17 Suppl 5 Improving, S146–53. [PubMed: 21761953]

Bergers E, Bot JCJ, Groot CJAD, Polman CH, Nijeholt GJL à Castelijns JA, Valk P. van der, Barkhof F, 2002. Axonal damage in the spinal cord of MS patients occurs largely independent of T2 MRI lesions. Neurology 59, 1766–1771. 10.1212/01.WNL.0000036566.00866.26 [PubMed: 12473766]

Bester M, Jensen JH, Babb JS, Tabesh A, Miles L, Herbert J, Grossman RI, Inglese M, 2015. Non-Gaussian diffusion MRI of gray matter is associated with cognitive impairment in multiple sclerosis. Mult Scler 21, 935–944. 10.1177/1352458514556295 [PubMed: 25392318]

Biton IE, Mayk A, Kidron D, Assaf Y, Cohen Y, 2005. Improved detectability of experimental allergic encephalomyelitis in excised swine spinal cords by high b-value q-space DWI. Experimental Neurology 195, 437–446. 10.1016/j.expneurol.2005.06.011 [PubMed: 16098966]

Bodini B, Khaleeli Z, Cercignani Mara, Miller David H., Thompson Alan J., Ciccarelli Olga, 2009. Exploring the relationship between white matter and gray matter damage in early primary progressive multiple sclerosis: An in vivo study with TBSS and VBM. Human Brain Mapping 30, 2852–2861. 10.1002/hbm.20713 [PubMed: 19172648]

Bolker BM, Brooks ME, Clark CJ, Geange SW, Poulsen JR, Stevens MHH, White J-SS, 2009. Generalized linear mixed models: a practical guide for ecology and evolution. Trends in Ecology & Evolution 24, 127–135. 10.1016/j.tree.2008.10.008 [PubMed: 19185386]

Budde MD, Xie M, Cross AH, Song S-K, 2009. Axial Diffusivity Is the Primary Correlate of Axonal Injury in the Experimental Autoimmune Encephalomyelitis Spinal Cord: A Quantitative Pixelwise Analysis. J. Neurosci. 29, 2805–2813. 10.1523/JNEUROSCI.4605-08.2009 [PubMed: 19261876]

By S, Xu J, Box BA, Bagnato FR, Smith SA, 2018. Multi-compartmental diffusion characterization of the human cervical spinal cord in vivo using the spherical mean technique. NMR in Biomedicine 31, e3894. 10.1002/nbm.3894 [PubMed: 29388719]

By S, Xu J, Box BA, Bagnato FR, Smith SA, 2017. Application and evaluation of NODDI in the cervical spinal cord of multiple sclerosis patients. NeuroImage: Clinical 15, 333–342. 10.1016/j.nicl.2017.05.010 [PubMed: 28560158]

Ceccarelli A, Rocca MA, Falini A, Tortorella P, Pagani E, Rodegher M, Comi G, Scotti G, Filippi M, 2007. Normal-appearing white and grey matter damage in MS. J Neurol 254, 513–518. 10.1007/s00415-006-0408-4 [PubMed: 17401516]

Chuhutin A, Hansen B, Jespersen SN, 2017. Precision and accuracy of diffusion kurtosis estimation and the influence of b-value selection. NMR in Biomedicine 30, e3777. 10.1002/nbm.3777

Coelho S, Pozo JM, Jespersen SN, Jones DK, Frangi AF, 2019. Resolving degeneracy in diffusion MRI biophysical model parameter estimation using double diffusion encoding. Magnetic Resonance in Medicine 82, 395–410. 10.1002/mrm.27714 [PubMed: 30865319]

Cohen Y, Anaby D, Morozov D, 2016. Diffusion MRI of the spinal cord: from structural studies to pathology. NMR in Biomedicine 30, e3592. 10.1002/nbm.3592

Compston A, Coles A, 2002. Multiple sclerosis. Lancet 359, 1221–1231. 10.1016/S0140-6736(02)08220-X [PubMed: 11955556]

de Kouchkovsky I, Fieremans E, Fleysher L, Herbert J, Grossman RI, Inglese M, 2016. Quantification of normal-appearing white matter tract integrity in multiple sclerosis: a diffusion kurtosis imaging study. Journal of Neurology 263, 1146–1155. 10.1007/s00415-016-8118-z [PubMed: 27094571]

De Santis S, Jones DK, Roebroeck A, 2016. Including diffusion time dependence in the extra-axonal space improves in vivo estimates of axonal diameter and density in human white matter. NeuroImage 130, 91–103. 10.1016/j.neuroimage.2016.01.047 [PubMed: 26826514]

De Stefano N, Battaglini M, Stromillo ML, Zipoli V, Bartolozzi ML, Guidi L, Siracusa G, Portaccio E, Giorgio A, Sorbi S, Federico A, Amato MP, 2006. Brain damage as detected by magnetization transfer imaging is less pronounced in benign than in early relapsing multiple sclerosis. Brain 129, 2008–2016. 10.1093/brain/awl152 [PubMed: 16815879]

Delgado y Palacios R, Verhoye M, Henningsen K, Wiborg O, der Linden AV, 2014. Diffusion Kurtosis Imaging and High-Resolution MRI Demonstrate Structural Aberrations of Caudate Putamen and Amygdala after Chronic Mild Stress. PLOS ONE 9, e95077. 10.1371/journal.pone.0095077 [PubMed: 24740310]

Dyrby TB, S-gaard LV, Hall MG, Ptito M, Alexander Daniel.C., 2013. Contrast and stability of the axon diameter index from microstructure imaging with diffusion MRI. Magnetic Resonance in Medicine 70, 711–721. 10.1002/mrm.24501 [PubMed: 23023798]

Edwards LJ, Muller KE, Wolfinger RD, Qaqish BF, Schabenberger O, 2008. An R2 statistic for fixed effects in the linear mixed model. Statistics in Medicine 27, 6137–6157. 10.1002/sim.3429 [PubMed: 18816511]

Evangelou N, Esiri MM, Smith S, Palace J, Matthews PM, 2000. Quantitative pathological evidence for axonal loss in normal appearing white matter in multiple sclerosis. Ann Neurol. 47, 391–395. 10.1002/1531-8249(200003)47:3<391::AID-ANA20>3.0.CO;2-J [PubMed: 10716264]

Falangola MF, Guilfoyle DN, Tabesh A, Hui ES, Nie X, Jensen JH, Gerum SV, Hu C, LaFrancois J, Collins HR, Helpern JA, 2014. Histological correlation of diffusional kurtosis and white matter modeling metrics in cuprizone-induced corpus callosum demyelination. NMR Biomed. 27, 948–957. 10.1002/nbm.3140 [PubMed: 24890981]

Fieremans E, Jensen JH, Helpern JA, 2011. White matter characterization with diffusional kurtosis imaging. NeuroImage 58, 177–188. 10.1016/j.neuroimage.2011.06.006 [PubMed: 21699989]

Fieremans E, Jensen JH, Helpern JA, Kim S, Grossman RI, Inglese M, Novikov DS, 2012. Diffusion distinguishes between axonal loss and demyelination in brain white matter, in: 20th Annual Meeting of the International Society for Magnetic Resonance in Medicine. Melbourne, Australia. p. 465.

Filippi M, Rocca MA, 2011. MR imaging of multiple sclerosis. Radiology 259, 659–681. 10.1148/radiol.11101362 [PubMed: 21602503]

Filippi M, Rocca MA, Barkhof F, Brück W, Chen JT, Comi G, DeLuca G, De Stefano N, Erickson BJ, Evangelou N, Fazekas F, Geurts JJ, Lucchinetti C, Miller DH, Pelletier D, Popescu BFG, Lassmann H, 2012. Association between pathological and MRI findings in multiple sclerosis. The Lancet Neurology 11, 349–360. 10.1016/S1474-4422(12)70003-0 [PubMed: 22441196]

Filli L, Wurnig M, Nanz D, Luechinger R, Kenkel D, Boss A, 2014. Whole-Body Diffusion Kurtosis Imaging: Initial Experience on Non-Gaussian Diffusion in Various Organs. Investigative Radiology 49, 773. 10.1097/RLI.0000000000000082 [PubMed: 24979203]

Gelman A, Hill J, 2007. Data analysis using regression and multilevel/hierarchical models. Cambridge University Press, Cambridge; New York.

Goldstein H, 2011. Multilevel statistical models, 4th ed. ed, Wiley series in probability and statistics. Wiley, Chichester, West Sussex.

Grossman EJ, Ge Y, Jensen JH, Babb JS, Miles L, Reaume J, Silver JM, Grossman RI, Inglese M, 2011. Thalamus and Cognitive Impairment in Mild Traumatic Brain Injury: A Diffusional Kurtosis Imaging Study. Journal of Neurotrauma 29, 2318–2327. 10.1089/neu.2011.1763 [PubMed: 21639753]

Grussu F, Schneider T, Tur C, Tachrount Mohamed, Ianuş Andrada, Yiannakas Marios C., Newcombe Jia, Zhang Hui, Alexander Daniel C., DeLuca Gabriele C., Gandini Wheeler-Kingshott Claudia A. M., 2017. Neurite dispersion: a new marker of multiple sclerosis spinal cord pathology? Annals of Clinical and Translational Neurology 4, 663–679. 10.1002/acn3.445 [PubMed: 28904988]

Grussu F, Schneider T, Zhang H, Alexander DC, Wheeler–Kingshott CAM, 2015. Neurite orientation dispersion and density imaging of the healthy cervical spinal cord in vivo. NeuroImage 111, 590–601. 10.1016/j.neuroimage.2015.01.045 [PubMed: 25652391]

Guglielmetti C, Veraart J, Roelant E, Mai Z, Daans J, Van Audekerke J, Naeyaert M, Vanhoutte G, Delgado y Palacios R, Praet J, Fieremans E, Ponsaerts P, Sijbers J, Van der Linden A, Verhoye M, 2016. Diffusion kurtosis imaging probes cortical alterations and white matter pathology following cuprizone induced demyelination and spontaneous remyelination. NeuroImage 125, 363–377. 10.1016/j.neuroimage.2015.10.052 [PubMed: 26525654]

Hansen B, Jespersen SN, 2017. Recent Developments in Fast Kurtosis Imaging. Front. Phys 5. 10.3389/fphy.2017.00040

Hansen B, Jespersen SN, 2016. Kurtosis fractional anisotropy, its contrast and estimation by proxy. Scientific Reports 6, 23999. 10.1038/srep23999 [PubMed: 27041679]

Hansen B, Khan AR, Shemesh N, Lund TE, Sangill R, Eskildsen SF, Østergaard L, Jespersen SN, 2017. White matter biomarkers from fast protocols using axially symmetric diffusion kurtosis imaging. NMR in Biomedicine 30, e3741. 10.1002/nbm.3741

Hansen B, Lund TE, Sangill R, Jespersen SN, 2014. Erratum: Hansen, Lund, Sangill, and Jespersen. Experimentally and Computationally Fast Method for Estimation of a Mean Kurtosis. Magnetic Resonance in Medicine 69:1754–1760 (2013). Magnetic Resonance in Medicine 71, 2250–2250. 10.1002/mrm.25090

Hansen B, Lund TE, Sangill R, Jespersen SN, 2013. Experimentally and computationally fast method for estimation of a mean kurtosis. Magn Reson Med 69, 1754–1760. 10.1002/mrm.24743 [PubMed: 23589312]

Hansen B, Shemesh N, Jespersen SN, 2016. Fast imaging of mean, axial and radial diffusion kurtosis. NeuroImage 142, 381–393. 10.1016/j.neuroimage.2016.08.022 [PubMed: 27539807]

Hori M, Tsutsumi S, Yasumoto Y, Ito M, Suzuki M, Tanaka FS, Kyogoku S, Nakamura M, Tabuchi T, Fukunaga I, Suzuki Y, Kamagata K, Masutani Y, Aoki S, 2014. Cervical spondylosis: Evaluation of microstructural changes in spinal cord white matter and gray matter by diffusional kurtosis imaging. Magnetic Resonance Imaging 32, 428–432. 10.1016/j.mri.2014.01.018 [PubMed: 24602824]

Horowitz A, Barazany D, Tavor I, Yovel G, Assaf Y, 2015. Response to the comments on the paper by Horowitz et al.(2014). Brain Structure and Function 220, 1791. [PubMed: 25809450]

Hui ES, Fieremans E, Jensen JH, Tabesh A, Feng W, Bonilha L, Spampinato MV, Adams R, Helpern JA, 2012. Stroke Assessment With Diffusional Kurtosis Imaging. Stroke 43, 2968–2973. 10.1161/STROKEAHA.112.657742 [PubMed: 22933581]

Hui ES, Russell Glenn G, Helpern JA, Jensen JH, 2015. Kurtosis analysis of neural diffusion organization. NeuroImage 106, 391–403. 10.1016/j.neuroimage.2014.11.015 [PubMed: 25463453]

Inglese M, Bester M, 2010. Diffusion imaging in multiple sclerosis: research and clinical implications. NMR Biomed 23, 865–872. 10.1002/nbm.1515 [PubMed: 20882528]

Jelescu IO, Veraart J, Adisetiyo V, Milla SS, Novikov DS, Fieremans E, 2015a. One diffusion acquisition and different white matter models: How does microstructure change in human early development based on WMTI and NODDI? NeuroImage 107, 242–256. 10.1016/j.neuroimage.2014.12.009 [PubMed: 25498427]

Jelescu IO, Veraart J, Fieremans E, Novikov DS, 2015b. Degeneracy in model parameter estimation for multi-compartmental diffusion in neuronal tissue. NMR in Biomedicine 29, 33–47. 10.1002/nbm.3450 [PubMed: 26615981]

Jelescu IO, Zurek M, Winters KV, Veraart J, Rajaratnam A, Kim NS, Babb JS, Shepherd TM, Novikov DS, Kim SG, Fieremans E, 2016. In vivo quantification of demyelination and recovery using compartment-specific diffusion MRI metrics validated by electron microscopy. NeuroImage 132, 104–114. 10.1016/j.neuroimage.2016.02.004 [PubMed: 26876473]

Jensen JH, Helpern JA, 2010. MRI quantification of non-Gaussian water diffusion by kurtosis analysis. NMR Biomed. 23, 698–710. 10.1002/nbm.1518 [PubMed: 20632416]

Jensen JH, Helpern JA, Ramani A, Lu H, Kaczynski K, 2005. Diffusional kurtosis imaging: The quantification of non-gaussian water diffusion by means of magnetic resonance imaging. Magn. Reson. Med. 53, 1432–1440. 10.1002/mrm.20508 [PubMed: 15906300]

Jespersen SN, Kroenke CD, Østergaard L, Ackerman JJH, Yablonskiy DA, 2007. Modeling dendrite density from magnetic resonance diffusion measurements. NeuroImage 34, 1473–1486. 10.1016/j.neuroimage.2006.10.037 [PubMed: 17188901]

Jespersen SN, Leigland LA, Cornea A, Kroenke CD, 2012. Determination of Axonal and Dendritic Orientation Distributions Within the Developing Cerebral Cortex by Diffusion Tensor Imaging. IEEE Trans. Med. Imaging 31, 16–32. 10.1109/tmi.2011.2162099 [PubMed: 21768045]

Jespersen SN, Olesen JL, Hansen B, Shemesh N, 2017. Diffusion time dependence of microstructural parameters in fixed spinal cord. NeuroImage 10.1016/j.neuroimage.2017.08.039

Johnson PC, 2014. Extension of Nakagawa & Schielzeth's R2GLMM to random slopes models. Methods Ecol Evol 5, 944–946. 10.1111/2041-210X.12225 [PubMed: 25810896]

Kellner E, Dhital B, Kiselev VG, Reisert M, 2015. Gibbs-ringing artifact removal based on local subvoxel-shifts. Magnetic Resonance in Medicine 76, 1574–1581. 10.1002/mrm.26054 [PubMed: 26745823]

Kelm ND, West KL, Carson RP, Gochberg DF, Ess KC, Does MD, 2016. Evaluation of diffusion kurtosis imaging in ex vivo hypomyelinated mouse brains. NeuroImage 124, Part A, 612–626. 10.1016/j.neuroimage.2015.09.028 [PubMed: 26400013]

Khan AR, 2016. Chronic Mild Stress Induces Changes in Neurite Density in the Amygdala as Revealed by Diffusion MRI and Validated with Novel Histological Analyses.

Kipp M, Nyamoya S, Hochstrasser T, Amor S, 2016. Multiple sclerosis animal models: a clinical and histopathological perspective. Brain Pathology 27, 123–137. 10.1111/bpa.12454

Kiselev VG, 2010. The Cumulant Expansion: An Overarching Mathematical Framework For Understanding Diffusion NMR, in: Jones DK (Ed.), Diffusion MRI Oxford University Press, pp. 152–168.

Klawiter EC, Schmidt RE, Trinkaus K, Liang H-F, Budde MD, Naismith RT, Song S-K, Cross AH, Benzinger TL, 2011. Radial diffusivity predicts demyelination in ex vivo multiple sclerosis spinal cords. NeuroImage 55, 1454–1460. 10.1016/j.neuroimage.2011.01.007 [PubMed: 21238597]

Kunz N, da Silva AR, Jelescu IO, 2018. Intra- and extra-axonal axial diffusivities in the white matter: Which one is faster? NeuroImage 181, 314–322. 10.1016/j.neuroimage.2018.07.020 [PubMed: 30005917]

Lampinen B, Szczepankiewicz F, Novén M, van Westen D, Hansson O, Englund E, Mårtensson J, Westin C-F, Nilsson M, 2018. Can the neurite density be estimated with diffusion MRI? A multidimensional MRI study using b-tensor encoding and multiple echo times. arXiv:1806.02731 [physics].

Lampinen B, Szczepankiewicz F, Novén M, van Westen D, Hansson O, Englund E, Mårtensson J, Westin C-F, Nilsson M, 2019. Searching for the neurite density with diffusion MRI: Challenges for biophysical modeling. Human Brain Mapping 40, 2529–2545. 10.1002/hbm.24542 [PubMed: 30802367]

Lassmann H, Bradl M, 2016. Multiple sclerosis: experimental models and reality. Acta Neuropathol 1–22. 10.1007/s00401-016-1631-4

Li D, Wang X, 2017. Application value of diffusional kurtosis imaging (DKI) in evaluating microstructural changes in the spinal cord of patients with early cervical spondylotic myelopathy. Clinical Neurology and Neurosurgery 156, 71–76. 10.1016/j.clineuro.2017.03.015 [PubMed: 28349894]

Lin X, Tench CR, Evangelou N, Jaspan T, Constantinescu SC, 2006. Measurement of Spinal Cord Atrophy in Multiple Sclerosis. Journal of Neuroimaging 14, 20S–26S. 10.1111/j.1552-6569.2004.tb00275.x

Mesaros S, Rocca MA, Riccitelli G, Pagani E, Rovaris M, Caputo D, Ghezzi A, Capra R, Bertolotto A, Comi G, Filippi M, 2009. Corpus callosum damage and cognitive dysfunction in benign MS. Hum. Brain Mapp 30, 2656–2666. 10.1002/hbm.20692 [PubMed: 19067325]

Miller DH, Thompson AJ, Filippi M, 2003. Magnetic resonance studies of abnormalities in the normal appearing white matter and grey matter in multiple sclerosis. J Neurol 250, 1407–1419. 10.1007/s00415-003-0243-9 [PubMed: 14673572]

Naismith RT, Xu J, Tutlam NT, Scully PT, Trinkaus K, Snyder AZ, Song S-K, Cross AH, 2010. Increased diffusivity in acute multiple sclerosis lesions predicts risk of black hole. Neurology 74, 1694. 10.1212/WNL.0b013e3181e042c4 [PubMed: 20498437]

Nakagawa S, Schielzeth H, O'Hara RB, 2013. A general and simple method for obtaining R2 from generalized linear mixed-effects models. Methods in Ecology and Evolution 4, 133–142. 10.1111/j.2041-210x.2012.00261.x

Nathoo N, Yong VW, Dunn JF, 2014. Understanding disease processes in multiple sclerosis through magnetic resonance imaging studies in animal models. NeuroImage: Clinical 4, 743–756. 10.1016/j.nicl.2014.04.011 [PubMed: 24936425]

Nilsson M, Lasič S, Drobnjak I, Topgaard D, Westin C-F, 2017. Resolution limit of cylinder diameter estimation by diffusion MRI: The impact of gradient waveform and orientation dispersion. NMR in Biomedicine 30, e3711. 10.1002/nbm.3711

Nilsson M, Lätt J, Nordh E, Wirestam R, Ståhlberg F, Brockstedt S, 2009. On the effects of a varied diffusion time in vivo: is the diffusion in white matter restricted? Magnetic Resonance Imaging 27, 176–187. 10.1016/j.mri.2008.06.003 [PubMed: 18657924]

Nilsson M, van Westen D, Ståhlberg F, Sundgren PC, Lätt J, 2013. The role of tissue microstructure and water exchange in biophysical modelling of diffusion in white matter. MAGMA 26, 345–370. 10.1007/s10334-013-0371-x [PubMed: 23443883]

Novikov DS, Jespersen SN, Kiselev VG, Fieremans E, 2016. Quantifying brain microstructure with diffusion MRI: Theory and parameter estimation. arXiv:1612.02059 [physics].

Novikov DS, Kiselev VG, 2010. Effective medium theory of a diffusion-weighted signal. NMR Biomed. 23, 682–697. 10.1002/nbm.1584 [PubMed: 20886563]

Novikov DS, Kiselev VG, Jespersen SN, 2018a. On modeling. Magnetic Resonance in Medicine 79, 3172–3193. 10.1002/mrm.27101 [PubMed: 29493816]

Novikov DS, Veraart J, Jelescu IO, Fieremans E, 2018b. Rotationally-invariant mapping of scalar and orientational metrics of neuronal microstructure with diffusion MRI. NeuroImage 174, 518–538. 10.1016/j.neuroimage.2018.03.006 [PubMed: 29544816]

Noyes K, Weinstock-Guttman B, 2013. Impact of diagnosis and early treatment on the course of multiple sclerosis. Am J Manag Care 19, s321–331. [PubMed: 24494633]

Ong HH, Wright AC, Wehrli SL, Souza A, Schwartz ED, Hwang SN, Wehrli FW, 2008. Indirect measurement of regional axon diameter in excised mouse spinal cord with q-space imaging: Simulation and experimental studies. NeuroImage 40, 1619–1632. 10.1016/j.neuroimage.2008.01.017 [PubMed: 18342541]

Pirko I, Lucchinetti CF, Sriram S, Bakshi R, 2007. Gray matter involvement in multiple sclerosis. Neurology 68, 634. 10.1212/01.wnl.0000250267.85698.7a [PubMed: 17325269]

Polman CH, Reingold SC, Banwell B, Clanet Michel, Cohen Jeffrey A., Filippi Massimo, Fujihara Kazuo, Havrdova Eva, Hutchinson Michael, Kappos Ludwig, Lublin Fred D., Montalban Xavier, O'Connor Paul, Sandberg-Wollheim Magnhild, Thompson Alan J., Waubant Emmanuelle, Weinshenker Brian, Wolinsky Jerry S., 2011. Diagnostic criteria for multiple sclerosis: 2010 Revisions to the McDonald criteria. Annals of Neurology 69, 292–302. 10.1002/ana.22366 [PubMed: 21387374]

Raz E, Bester M, Sigmund EE, Tabesh A, Babb JS, Jaggi H, Helpern J, Mitnick RJ, Inglese M, 2013. A Better Characterization of Spinal Cord Damage in Multiple Sclerosis: A Diffusional Kurtosis Imaging Study. AJNR Am J Neuroradiol 34, 1846–1852. 10.3174/ajnr.A3512 [PubMed: 23578677]

Reisert M, Kiselev VG, Dhital B, 2019. A unique analytical solution of the white matter standard model using linear and planar encodings. Magnetic Resonance in Medicine 81, 3819–3825. 10.1002/mrm.27685 [PubMed: 30809854]

Robinson KM, Njus JM, Phillips DA, Proctor TM, Rooney WD, Jones RE, 2010. MR Imaging of Inflammation during Myelin-Specific T Cell-Mediated Autoimmune Attack in the EAE Mouse Spinal Cord. Mol Imaging Biol 12, 240–249. 10.1007/s11307-009-0272-6 [PubMed: 19949987]

Rosenkrantz AB, Padhani AR, Chenevert TL, Koh D-M, Keyzer FD, Taouli B, Bihan DL, 2015. Body diffusion kurtosis imaging: Basic principles, applications, and considerations for clinical practice. Journal of Magnetic Resonance Imaging 42, 1190–1202. 10.1002/jmri.24985 [PubMed: 26119267]

Sathornsumetee S, McGavern DB, Ure DR, Rodriguez M, 2000. Quantitative Ultrastructural Analysis of a Single Spinal Cord Demyelinated Lesion Predicts Total Lesion Load, Axonal Loss, and Neurological Dysfunction in a Murine Model of Multiple Sclerosis. The American Journal of Pathology 157, 1365–1376. 10.1016/S0002-9440(10)64650-0 [PubMed: 11021839]

Schneider T, Brownlee W, Zhang H, Ciccarelli O, Miller DH, Wheeler-Kingshott CG, 2017. Sensitivity of multi-shell NODDI to multiple sclerosis white matter changes: a pilot study. Funct Neurol 32, 97–101. 10.11138/FNeur/2017.32.2.097 [PubMed: 28676143]

Shepherd TM, Thelwall PE, Stanisz GJ, Blackband SJ, 2009. Aldehyde fixative solutions alter the water relaxation and diffusion properties of nervous tissue. Magnetic Resonance in Medicine 62, 26–34. 10.1002/mrm.21977 [PubMed: 19353660]

Shepherd TM, Thelwall PE, Stanisz GJ, Blackband SJ, 2005. Chemical fixation alters the water microenvironment in rat cortical brain slices—implications for MRI contrast mechanisms, in: Proc. Int. Soc. Magn. Reson. Med p. 619.

Steenwijk MD, Daams M, Pouwels PJW, Balk LJ, Tewarie PK, Geurts JJG, Barkhof F, Vrenken H, 2015. Unraveling the relationship between regional gray matter atrophy and pathology in connected white matter tracts in long-standing multiple sclerosis. Human Brain Mapping 36, 1796–1807. 10.1002/hbm.22738 [PubMed: 25627545]

Steinbrecher A, Weber T, Neuberger T, Mueller AM, Pedré X, Giegerich G, Bogdahn U, Jakob P, Haase A, Faber C, 2005. Experimental Autoimmune Encephalomyelitis in the Rat Spinal Cord: Lesion Detection with High-Resolution MR Microscopy at 17.6 T. American Journal of Neuroradiology 26, 19–25. [PubMed: 15661692]

Sun S-W, Neil JJ, Liang H-F, He YY, Schmidt RE, Hsu CY, Song S-K, 2005. Formalin fixation alters water diffusion coefficient magnitude but not anisotropy in infarcted brain. Magnetic Resonance in Medicine 53, 1447–1451. 10.1002/mrm.20488 [PubMed: 15906292]

Surova Y, Lampinen B, Nilsson M, Lätt J, Hall S, Widner H, Study SB, van Westen D, Hansson O, 2016. Alterations of Diffusion Kurtosis and Neurite Density Measures in Deep Grey Matter and White Matter in Parkinson's Disease. PLOS ONE 11, e0157755. 10.1371/journal.pone.0157755 [PubMed: 27362763]

Szczepankiewicz F, van Westen D, Englund E, Westin C-F, Ståhlberg F, Lätt J, Sundgren PC, Nilsson M, 2016. The link between diffusion MRI and tumor heterogeneity: Mapping cell eccentricity and density by diffusional variance decomposition (DIVIDE). NeuroImage 142, 522–532. 10.1016/j.neuroimage.2016.07.038 [PubMed: 27450666]

Tewarie P, Steenwijk MD, Brookes MJ, Uitdehaag BMJ, Geurts JJG, Stam CJ, Schoonheim MM, 2018. Explaining the heterogeneity of functional connectivity findings in multiple sclerosis: An empirically informed modeling study. Human Brain Mapping 39, 2541–2548. 10.1002/hbm.24020 [PubMed: 29468785]

Tietze A, Hansen MB, Østergaard L, Jespersen SN, Sangill R, Lund TE, Geneser M, Hjelm M, Hansen B, 2015. Mean Diffusional Kurtosis in Patients with Glioma: Initial Results with a Fast Imaging Method in a Clinical Setting. AJNR Am J Neuroradiol 36, 1472–1478. 10.3174/ajnr.A4311 [PubMed: 25977481]

Topfer R, Starewicz P, Lo K-M, Metzemaekers K, Jette D, Hetherington HP, Stikov N, Cohen-Adad J, 2016. A 24-channel shim array for the human spinal cord: Design, evaluation, and application. Magnetic Resonance in Medicine 76, 1604–1611. 10.1002/mrm.26354 [PubMed: 27487798]

Tremblay A, Tucker BV, 2011. The effects of N-gram probabilistic measures on the recognition and production of four-word sequences. The Mental Lexicon 6, 302–324. 10.1075/ml.6.2.04tre

van Kampen NG, 2007. Stochastic processes in physics and chemistry, 3rd ed. ed, North-Holland personal library. Elsevier, Amsterdam; Boston.

Veraart J, Fieremans E, Novikov DS, 2015. Diffusion MRI noise mapping using random matrix theory. Magnetic Resonance in Medicine 76, 1582–1593. 10.1002/mrm.26059 [PubMed: 26599599]

Veraart J, Poot DHJ, Van Hecke W, Blockx I, Van der Linden A, Verhoye M, Sijbers J, 2011. More accurate estimation of diffusion tensor parameters using diffusion kurtosis imaging. Magn. Reson. Med 65, 138–145. 10.1002/mrm.22603 [PubMed: 20878760]

Veraart J, Sijbers J, Sunaert S, Leemans A, Jeurissen B, 2013. Weighted linear least squares estimation of diffusion MRI parameters: Strengths, limitations, and pitfalls. NeuroImage 81, 335–346. 10.1016/j.neuroimage.2013.05.028 [PubMed: 23684865]

Wang J-J, Lin W-Y, Lu C-S, Weng Y-H, Ng S-H, Wang C-H, Liu H-L, Hsieh R-H, Wan Y-L, Wai Y-Y, 2011. Parkinson Disease: Diagnostic Utility of Diffusion Kurtosis Imaging. Radiology 261, 210–217. 10.1148/radiol.11102277 [PubMed: 21771952]

Watson C (Ed.), 2009. The spinal cord: a Christopher and Dana Reeve Foundation text and atlas. Academic, London.

West KL, Kelm ND, Carson RP, Alexander DC, Gochberg DF, Does MD, 2018. Experimental studies of g-ratio MRI in ex vivo mouse brain. NeuroImage 167, 366–371. 10.1016/j.neuroimage.2017.11.064 [PubMed: 29208572]

Wheeler-Kingshott CA, Stroman PW, Schwab JM, Bacon M, Bosma R, Brooks J, Cadotte DW, Carlstedt T, Ciccarelli O, Cohen-Adad J, Curt A, Evangelou N, Fehlings MG, Filippi M, Kelley BJ, Kollias S, Mackay A, Porro CA, Smith S, Strittmatter SM, Summers P, Thompson AJ, Tracey I, 2014. The current state-of-the-art of spinal cord imaging: Applications. NeuroImage 84, 1082–1093. 10.1016/j.neuroimage.2013.07.014 [PubMed: 23859923]

Wilkinson GN, Rogers CE, 1973. Symbolic Description of Factorial Models for Analysis of Variance. Journal of the Royal Statistical Society. Series C (Applied Statistics) 22, 392–399. 10.2307/2346786

Wlodarczyk A, Løbner M, Cédile O, Owens T, 2014. Comparison of microglia and infiltrating CD11c+ cells as antigen presenting cells for T cell proliferation and cytokine response. Journal of Neuroinflammation 11, 57. 10.1186/1742-2094-11-57 [PubMed: 24666681]

Wu EX, Cheung MM, 2010. MR diffusion kurtosis imaging for neural tissue characterization. NMR in Biomedicine 23, 836–848. 10.1002/nbm.1506 [PubMed: 20623793]

Wuerfel J, Tysiak E, Prozorovski T, Smyth Maureen, Mueller Susanne, Schnorr Joerg, Taupitz Matthias, Zipp Frauke, 2007. Mouse model mimics multiple sclerosis in the clinico-radiological paradox. European Journal of Neuroscience 26, 190–198. 10.1111/j.1460-9568.2007.05644.x [PubMed: 17596194]

Yoshida M, Hori M, Yokoyama K, Fukunaga I, Suzuki M, Kamagata K, Shimoji K, Nakanishi A, Hattori N, Masutani Y, Aoki S, 2013. Diffusional kurtosis imaging of normal-appearing white matter in multiple sclerosis: preliminary clinical experience. Jpn J Radiol 31, 50–55. 10.1007/s11604-012-0147-7 [PubMed: 23086313]

Zackowski KM, Smith SA, Reich DS, Gordon-Lipkin E, Chodkowski BA, Sambandan DR, Shteyman M, Bastian AJ, Zijl V, C, P., Calabresi PA, 2009. Sensorimotor dysfunction in multiple sclerosis and column-specific magnetization transfer-imaging abnormalities in the spinal cord. Brain 132, 1200–1209. 10.1093/brain/awp032 [PubMed: 19297508]

Zhang H, Schneider T, Wheeler-Kingshott CA, Alexander DC, 2012. NODDI: Practical in vivo neurite orientation dispersion and density imaging of the human brain. NeuroImage 61, 1000–1016. 10.1016/j.neuroimage.2012.03.072 [PubMed: 22484410]

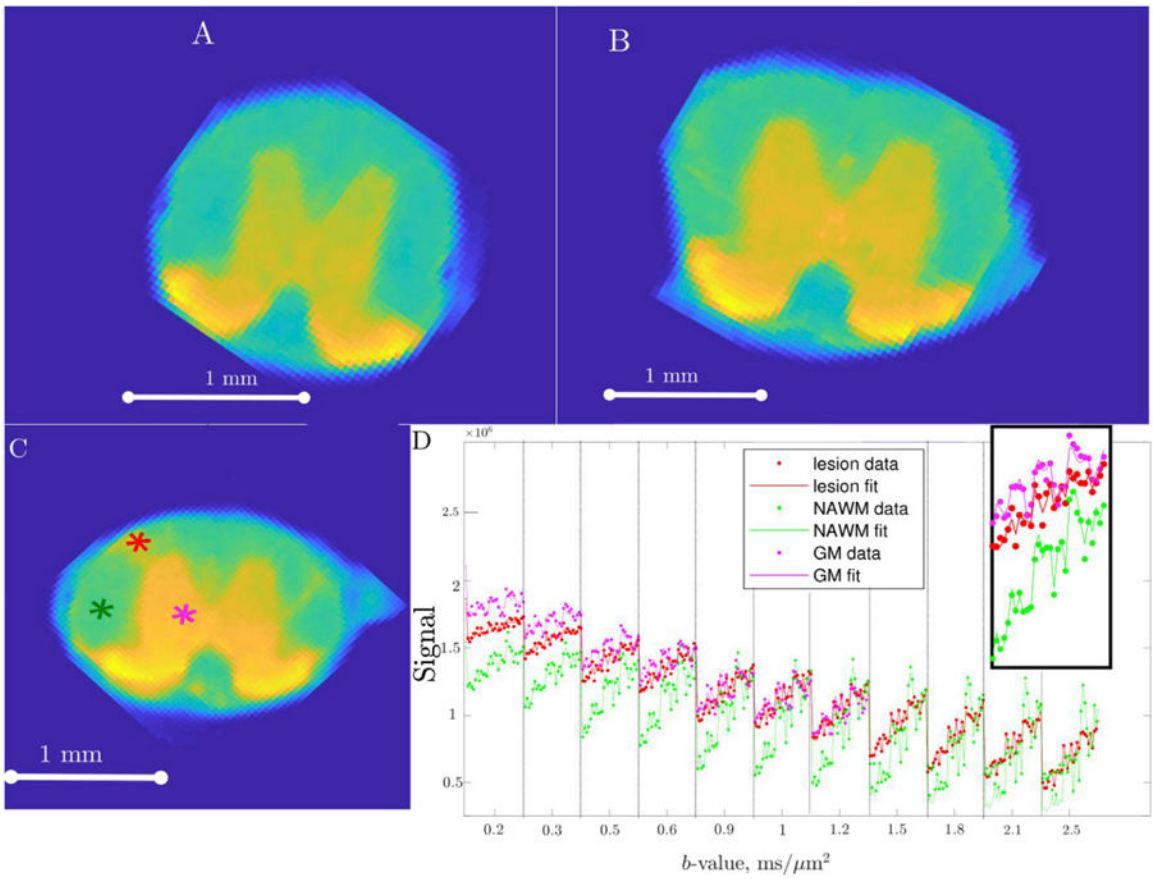

Fig. 1.

Example of acquired raw data and a corresponding data fit. Subfigures (A) and (B) show an example of a raw signal image acquired for low diffusion weighting (b=0.2 ms/μm^2) in mid thoracic and low thoracic segments of a control sample. Subfigure (C) shows a high grade sample, with a visible lesion acquired with the same low diffusion weighting (b=0.2 ms/μm^2). Data and data fit that correspond to three different voxels in the slice denoted in (C) are shown in subplot (D). Lesion voxel location is marked in red, NAWM voxel in green and GM voxel in magenta in subplot (C). Multiple data points plotted under each b-value on the x-axis correspond to different directions. The inset shows the enlarged part of the graph corresponding to b=0.5 ms/μm^2.

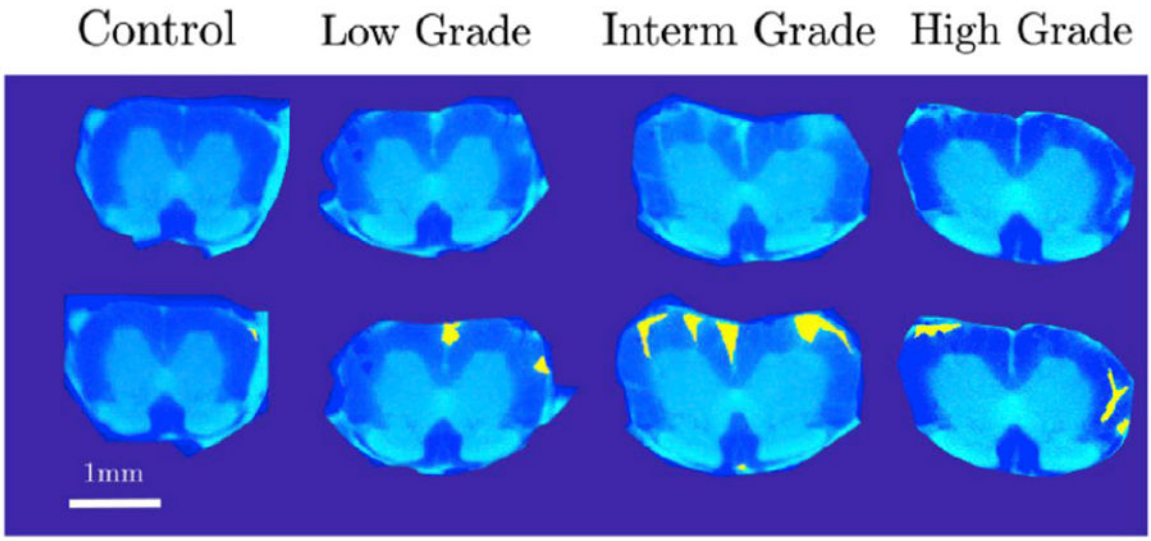

Fig. 2.

Example outcome of lesion identification in four spinal cords in a lumbar segment. From left to right the grades are control, low grade, intermediate grade and high grade of EAE. For each of two subplots, the upper image represents a raw T_2*-weighted image, while the lower image shows the same map with the manual lesion delineation superimposed in yellow.

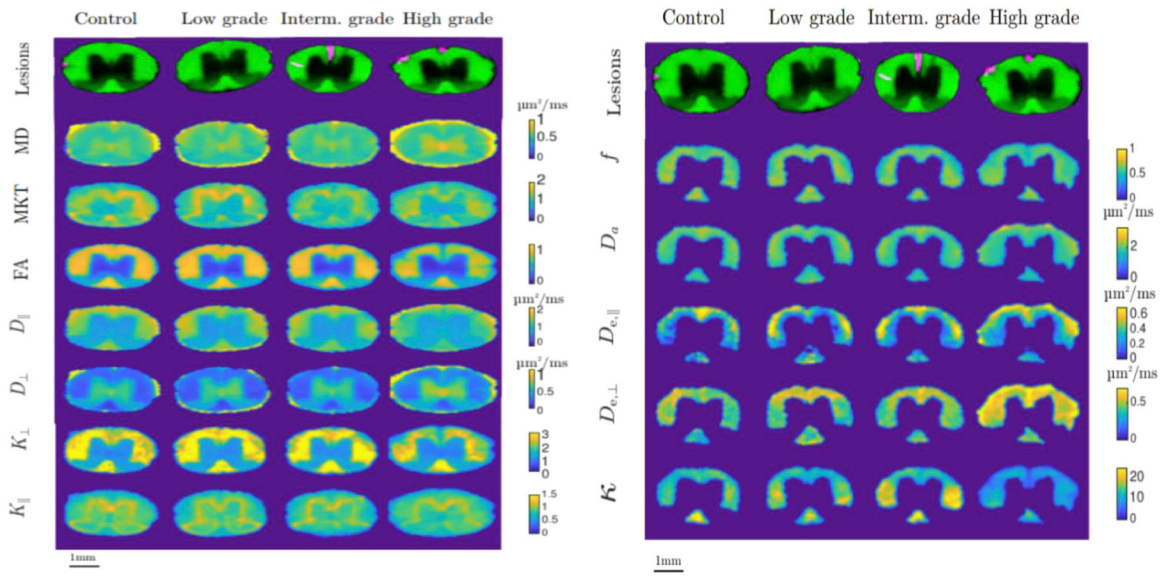

Fig. 3.

A: Examples of parameter maps for each of the measured parameters in mid-thoracic segments of spinal cord. Each column (from left to right) corresponds to different grades of EAE disability: control animal, low grade, intermediate grade and high grade of EAE. Rows correspond to different measured parameters (from top to bottom): mean diffusivity, MKT, FA, axial diffusivity, radial diffusivity, radial kurtosis, parallel kurtosis

B Examples of parameter maps for each of the measured parameters in mid-thoracic segments of spinal cord. Each column (from left to right) corresponds to different grades of EAE disability: control animal, low grade, intermediate grade and high grade of EAE. Rows correspond to different measured parameters: axonal water fraction, axonal diffusivity, axial extra-axonal diffusivity, radial extra-axonal diffusivity and concentration parameter of Watson distribution, the upper row depicts the delineation of spinal cord on the background of FA map.

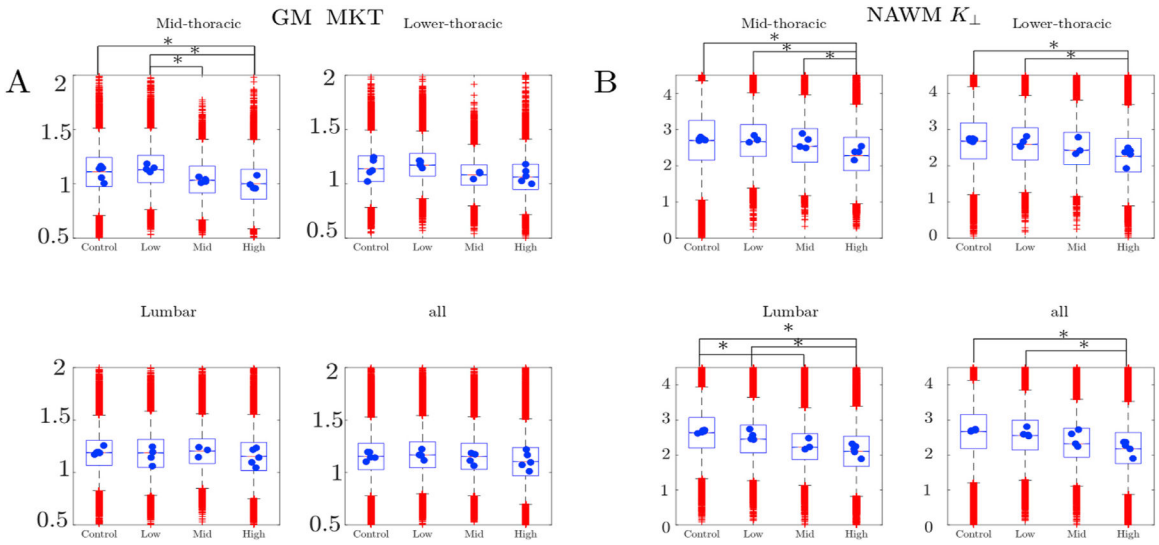

Fig. 4.

Examples of parameter distributions in the post-hoc parameter analysis for MKT in GM (A) and $K_\perp$ in NAWM (B) illustrated with box-plots. Each of 4 subplots corresponds to one of the spinal cord segments (mid-thoracic, low-thoracic and lumbar and a graph for all voxels pooled across segments). In each one of the subfigures a box-plot represents the distribution of values inside and outside the hyperintensity lesions. The outliers (voxels) are plotted individually as red crosses. Blue dots correspond to the parameter means within each spinal cord. Asterisk denotes significant group-wise difference between the spinal cord means. In all three plots the central mark indicates the data median, the bottom and top edges indicate the 25th and 75th percentiles. The whiskers extend to the most extreme data points excluding outliers.

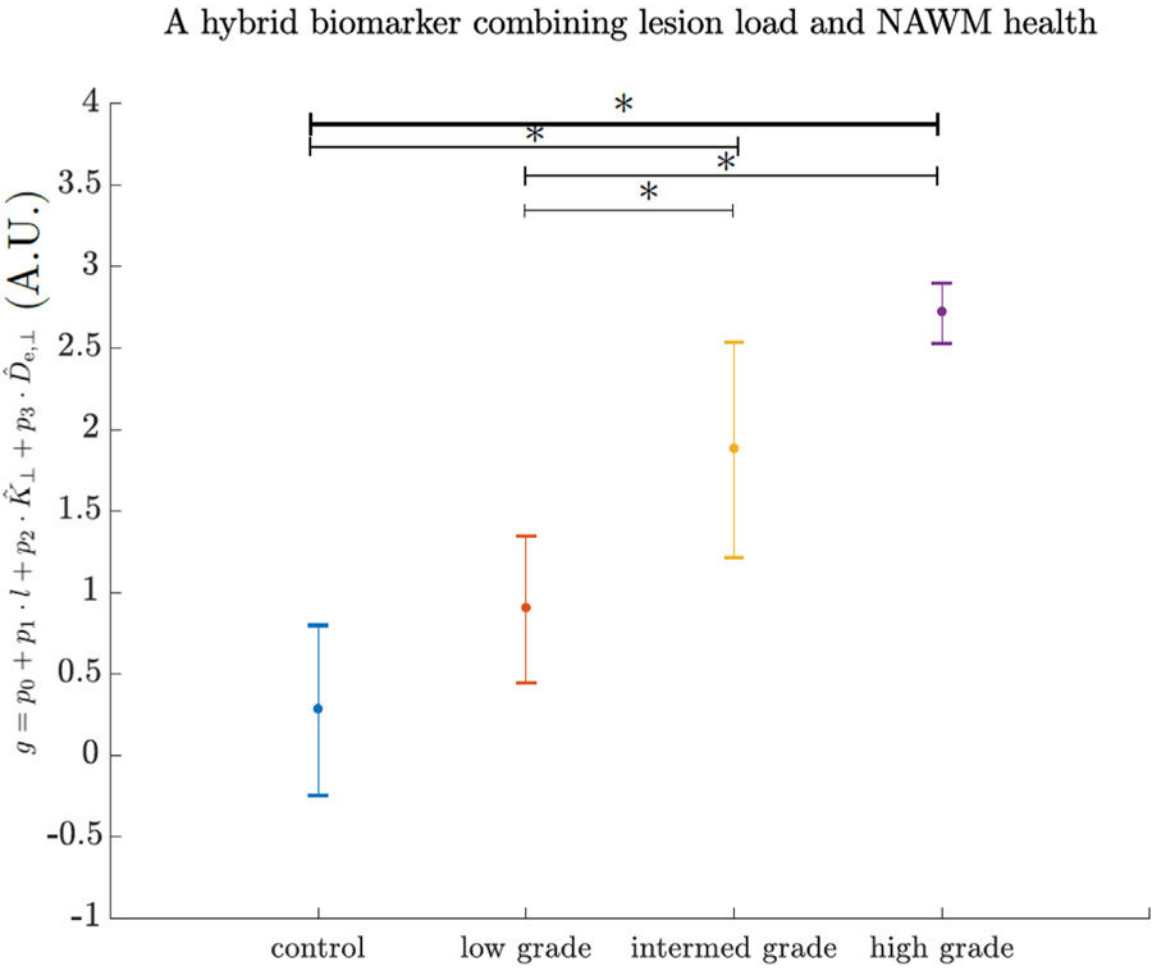

Fig. 5.

Application of a “hybrid” biomarker (Eq. 6) on animal-wise data. From left to right the values are group-wise means of described control, low-grade, intermediate and high grade EAE. Error bars depict standard deviation of animal-wise estimates of the biomarker. Asterisk denotes statistical significance measured with 1-way ANOVA.

Table 1:

Fit results of all measured parameters averaged for disability group. For each parameter a mean estimate provided along with standard deviation of error inside the lesion (subplot A) and outside the lesion (in NAWM, subplot B). The mean and standard deviation of error was calculated only in the tissues in which a particular parameter was used for a successive LME analysis. Thus the statistics for MKT and MD was estimated only in GM, and the statistics for the rest of the DKI and WMM parameters was estimated only in WM. Note also that GM parameters (MD,MKT) were not calculated inside the lesions.

A:Lesions

Tissue	Parameter	Control		Low grade		Intermed grade		High grade	
		Value	Stdev	Value	Stdev	Value	Stdev	Value	Stdev
GM	MD								
GM	MKT								
WM	$K_\perp$	1.89	0.52	1.44	0.46	1.37	0.37	1.37	0.43
WM	FA	0.48	0.17	0.35	0.15	0.35	0.11	0.40	0.14
WM	$K_\parallel$	1.04	0.17	0.96	0.14	0.89	0.12	0.94	0.12
WM	$D_\perp$	0.47	0.20	0.52	0.17	0.52	0.12	0.45	0.10
WM	$D_\parallel$	1.14	0.20	0.98	0.21	0.97	0.16	0.91	0.17
WM	f	0.54	0.08	0.51	0.09	0.49	0.07	0.48	0.08
WM	D_a	1.93	0.34	1.98	0.38	1.98	0.27	1.86	0.26
WM	$D_{e\parallel}$	0.45	0.18	0.50	0.25	0.55	0.18	0.49	0.17
WM	$D_{e\perp}$	0.66	0.22	0.78	0.23	0.74	0.16	0.64	0.15
WM	κ	5.31	2.58	3.83	2.04	3.52	1.83	4.08	1.96

B:NAWM

Tissue	Parameter	Control		Low grade		Intermed grade		High grade	
		Value	Stdev	Value	Stdev	Value	Stdev	Value	Stdev
GM	MD	0.57	0.06	0.58	0.06	0.58	0.06	0.58	0.07
GM	MKT	1.15	0.18	1.17	0.18	1.15	0.18	1.10	0.20
WM	$K_\perp$	2.66	0.71	2.57	0.65	2.36	0.64	2.20	0.67
WM	FA	0.80	0.06	0.79	0.07	0.74	0.10	0.74	0.11
WM	$K_\parallel$	0.91	0.14	0.87	0.13	0.89	0.14	0.87	0.15
WM	$D_\perp$	0.21	0.05	0.23	0.06	0.26	0.08	0.26	0.08

A:Lesions

Tissue	Parameter	Control		Low grade		Intermed grade		High grade	
		Value	Stdev	Value	Stdev	Value	Stdev	Value	Stdev
WM	$D_{\parallel}$	1.24	0.16	1.26	0.16	1.21	0.18	1.19	0.20
WM	f	0.64	0.07	0.64	0.06	0.61	0.06	0.61	0.07
WM	D_a	1.94	0.22	1.95	0.21	1.90	0.21	1.91	0.24
WM	$D_{e,\parallel}$	0.36	0.19	0.38	0.19	0.39	0.16	0.41	0.19
WM	$D_{e,\perp}$	0.48	0.12	0.49	0.11	0.54	0.12	0.49	0.13
WM	κ	12.54	3.92	12.67	4.17	9.90	3.88	10.82	4.55

Table 2:

The results of the fit of the linear mixed effects model. For each of the studied parameters (in rows), the following are presented in columns: percent of outlier values removed, quality of LME fit R^2_{β} (Edwards et al., 2008) p-values for coefficients of grade, lesion, segment and segment:lesion, partial $R^2_{\beta,\,p}$ (Edwards et al., 2008) of the same 4 coefficients and the results of the FDR multiple comparison test. Since lesions were registered only in WM, the coefficients of lesion are absent in GM.

Tissue	name	Outliers %	R^2_{β}	P-values				partial $R^2_{\beta,\,p}$				Grade FDR
				Grade	Lesion	Segment	Segment :Grade	Grade	Lesion	Segment	Segment Grade	
GM	MD	1.69	0.910	0.576		0.0598	0.382	0.117		0.588	0.295	
GM	MKT	1.80	0.980	0.010		0.136	0.290	0.863		0.710	0.663	*
WM	$K_{\perp}$	2.12	0.995	<0.001	<0.001	0.0111	0.004	0.953	0.991	0.896	0.839	*
WM	FA	3.50	0.977	0.042	<0.001	0.0023	0.004	0.852	0.982	0.972	0.852	
WM	$K_{\parallel}$	1.86	0.979	0.050	<0.001	<0.001	0.016	0.678	0.864	0.922	0.830	
WM	$D_{\perp}$	2.13	0.992	<0.001	<0.001	0.003	0.021	0.972	0.926	0.955	0.765	*
WM	$D_{\parallel}$	1.72	0.991	0.590	<0.001	0.0034	0.378	0.132	0.903	0.838	0.408	
WM	f	2.25	0.962	<0.001	<0.001	0.5822	0.011	0.967	0.971	0.259	0.853	*
WM	D_a	1.52	0.971	0.525	0.123	0.0127	0.110	0.204	0.478	0.862	0.543	
WM	$D_{e,\parallel}$	1.42	0.919	0.003	0.014	0.0044	0.349	0.886	0.738	0.923	0.412	*
WM	$D_{e,\perp}$	2.40	0.948	0.008	<0.001	0.0029	0.005	0.949	0.898	0.882	0.910	*
WM	κ	2.05	0.993	<0.001	<0.001	<0.001	<0.001	0.957	0.992	0.980	0.916	*

Table 3:

Post-hoc analysis of parameters in GM and NAWM. Average value for all the NAWM or GM in the particular segment in each sample. (A) For each of the disability groups comparisons low-grade vs intermediate grade, low-grade vs high grade and intermediate grade vs high grade parameters that were found significant ($p<0.05$) after ANOVA of per-sample mean in each one of the segments is provided in the corresponding cell. An FDR correction of multiple comparisons has been taken into account. GM parameters are underlined. (B) Each of disability groups (low, intermediate, high) compared with the control group. Parameters that were found significant ($p<0.05$) after ANOVA of per-sample mean in each of the segments are listed in corresponding cells. An FDR correction has been performed. GM parameters are underlined.

A

	Low grade	**Intermediate grade**	**High grade**
Low grade		MTO: <u>MKT</u>	MTO: <u>MKT</u>$K_\perp$ f $D_{e,\parallel}$ LTO: $K_\perp$ f LU: $K_\perp$ $D_\perp$ f All: $K_\perp$ f
Intermediate grade			MTO: $K_\perp$

B

	Low grade	**Intermediate grade**	**High grade**
Control	MTO:	MTO:	MTO: <u>MKT</u>$K_\perp$ f $D_{e,\parallel}$
	LTO:	LTO:	LTO: $K_\perp$ f $D_{e,\parallel}$
	LU:	LU: FA $K_\perp$ $D_\perp$ f	LU: FA $K_\perp$ $D_\perp$ f $D_{e,\parallel}$ κ
	All:	All: $D_{e,\parallel}$	All: $K_\perp$ $D_\perp$ f $D_{e,\parallel}$